

Repeater Swarm-Assisted Cellular Systems: Interaction Stability and Performance Analysis

Jianan Bai, Anubhab Chowdhury, Anders Hansson, and Erik G. Larsson

Abstract—We consider a cellular massive MIMO system where swarms of wireless repeaters are deployed to improve coverage. These repeaters are full-duplex relays with small form factors that receive and instantaneously retransmit signals. They can be deployed in a plug-and-play manner at low cost, while being transparent to the network—conceptually they are *active channel scatterers* with amplification capabilities. Two fundamental questions need to be addressed in repeater deployments: (i) How can we prevent destructive effects of positive feedback caused by inter-repeater interaction (i.e., each repeater receives and amplifies signals from others)? (ii) How much performance improvement can be achieved given that repeaters also inject noise and may introduce more interference? To answer these questions, we first derive a generalized Nyquist stability criterion for the repeater swarm system, and provide an easy-to-check stability condition. Then, we study the uplink performance and develop an efficient iterative algorithm that jointly optimizes the repeater gains, user transmit powers, and receive combining weights to maximize the weighted sum rate while ensuring system stability. Numerical results corroborate our theoretical findings and show that the repeaters can significantly improve the system performance, both in sub-6 GHz and millimeter-wave bands. The results also warrant careful deployment to fully realize the benefits of repeaters, for example, by ensuring a high probability of line-of-sight links between repeaters and the base station.

Index Terms—Repeaters, MIMO, positive feedback, stability, Nyquist criterion, performance analysis, optimization.

I. INTRODUCTION

Massive multiple-input multiple-output (MIMO), a key enabler for 5G cellular systems, provides high spectral efficiency and allows multiple users to be simultaneously served with low-complexity linear processing by deploying large antenna arrays at the base stations (BSs) [2]. However, cellular massive MIMO still suffers from poor cell-edge coverage due to severe signal attenuation and multi-cell interference. Additionally, the propagation environment in cellular networks is complex and there inevitably exist coverage holes due to shadowing and blockage. Furthermore, when supporting multi-antenna users, the channel rank deficiency, resulted from limited scattering, restricts the spatial multiplexing gains of massive MIMO.

A potential solution is distributed MIMO, also known as cell-free massive MIMO, where the antennas are grouped into many access points (APs), densely distributed across the coverage area [3]. In distributed MIMO systems, the likelihood

of a user being in the vicinity of some APs is significantly increased (a benefit known as macro diversity), effectively resolving the aforementioned issues. However, a widespread deployment of distributed MIMO is not yet practically viable, primarily due to the demanding requirements for high-capacity fronthaul, reciprocity calibration, and synchronization.

The limitation of cellular massive MIMO and the deployment challenges of distributed MIMO call for a transitional paradigm that retains the key benefits of distributed MIMO while minimizing deployment overhead. One promising solution is the repeater swarm-assisted cellular massive MIMO system conceptualized in [4], where large numbers (swarms) of repeaters are deployed within the cells to assist the signal propagation between the massive MIMO BSs and the users. These repeaters are essentially one type of full-duplex relays, amplifying and instantaneously retransmitting signals with minimal delay (less than a microsecond), and they can have very small form factors.

The use of repeaters as such is not a new concept—its commercial progress was initiated in 2G in order to improve coverage, especially in tunnels, and has been considered for various scenarios over the years [5]–[11]. In 5G New Radio (NR), significant efforts have been made to standardize network-controlled repeaters (NCRs) in 3GPP [12], enabling more functionalities through control signaling. The potential of NCRs has been demonstrated in many recent studies [13]–[23]. In this paper, we adopt the paradigm envisioned in [4], which differs slightly from the aforementioned works on multi-antenna NCRs: we consider simple single-antenna repeaters without beamforming capabilities, deployed in large numbers, densely within the cells. Conceptually, these repeaters function as *active channel scatterers* that amplify the signal. They can be deployed in a plug-and-play manner at very low cost, in a manner transparent to both the users and the BSs. Very few studies are available on the analysis and optimization of repeater swarms; an exception is [24] that considers repeater gain optimization for max-min fairness and energy efficiency; however, inter-repeater interaction (to be explained shortly) and user power control are not taken into account therein.

Meanwhile, several practical aspects of repeater deployment require careful consideration: in TDD operation they must be reciprocity calibrated [25]; they should have a linear time-invariant (LTI) response; be band-selective; offer enough self-interference mitigation; and have short delay. We refer to [4] for a detailed discussion of these properties.

Parts of the results in this paper were presented at IEEE SPAWC 2024 [1].

The authors are with the Department of Electrical Engineering (ISY), Linköping University, 58183 Linköping, Sweden (email: jianan.bai@liu.se, anuch87@liu.se, anders.g.hansson@liu.se, erik.g.larsson@liu.se). This work was supported in part by the Excellence Center at Linköping-Lund in Information Technology (ELLIIT), and by the Knut and Alice Wallenberg (KAW) foundation.

A. Two Fundamental Aspects

Most existing works on repeater-assisted cellular systems focus on numerical studies, lacking a comprehensive theoretical analysis. Additionally, inter-repeater interaction, a key factor that can cause system instability, is neglected in all literature we are aware of (except [1]). With this motivation, in this paper we investigate two fundamental aspects of repeater swarm-assisted cellular systems:

Interaction Stability: As repeaters operate in full-duplex, they inevitably pick up, amplify, and retransmit signals from each other. This creates a positive feedback loop within the repeater swarm, and this feedback loop can become unstable. (For analogy, imagine connecting a microphone to a speaker via an amplifier, and placing the microphone near the speaker: the microphone captures the sound from the speaker, amplifies and feeds it back to the speaker, causing a loud screech.) Theoretically, instability means unbounded growth of output power or energy; in practice, it leads to amplifier saturation and system malfunction. To prevent such issues, it is critical to identify conditions for system stability. To this end, we analyze repeater swarms from a linear system-theoretic perspective, and establish criteria for stability.

Communication Performance: Repeaters are not only signal amplifiers, but also active noise sources; the injected noise will be amplified along with the desired signals and received by the destination node. Meanwhile, as single-antenna devices without beamforming capabilities, repeaters cannot spatially separate signals. Especially in the uplink, signals from different users will be mixed at the repeaters, potentially causing severe interference. The performance of repeater swarm-assisted cellular systems is determined by a complex interplay between the signal amplification, noise injection, and interference mitigation. We develop a framework for quantifying the performance gains brought by repeater swarms in realistic scenarios.

B. Contributions and Organization of the Paper

- 1) In Section III, we introduce the system and signal model of a repeater swarm-assisted massive MIMO system. Particularly, the inter-repeater interaction is characterized and incorporated in this model.
- 2) We analyze the stability of repeater swarm systems in Section IV. Specifically, we derive a generalized Nyquist stability criterion for the system, and provide two sufficient conditions that are easy to verify in practice. The effectiveness of the derived conditions is then demonstrated through several examples.
- 3) The uplink performance of repeater swarm-assisted massive MIMO system is studied in Section V, in terms of the sum capacity and achievable rate under linear combining. We develop an efficient iterative algorithm to jointly optimize the repeater gains, user transmit powers, and receive combining weights, to maximize the weighted sum rate while ensuring system stability.
- 4) We present numerical results in Section VI, illustrating the performance gains brought by repeaters in both sub-6

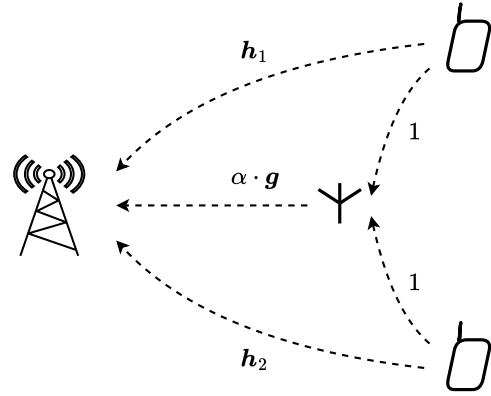


Fig. 1: A motivating example.

GHz and millimeter-wave bands. We also provide practical insights into repeater deployment.

This paper is a comprehensive extension of our conference paper [1], which contained a special case of the interaction stability analysis. Herein we develop a general framework for performance analysis, extend the stability analysis to arbitrary amplification gains, and provide a rigorous proof of the stability criterion stated in [1].

Notation: Time functions are written in Helvetica font, $x(t)$, and Laplace transforms in Italic font, $x(s)$. Vectors and matrices are written in boldface lowercase and uppercase, \mathbf{x} and \mathbf{X} , respectively. The determinant of \mathbf{X} is denoted $\det(\mathbf{X})$. $(\cdot)^T$, $(\cdot)^H$, and $(\cdot)^{-1}$ denote transpose, Hermitian (conjugate transpose), and inverse, respectively. \mathbf{I}_N and $\mathbf{0}_N$ denote the identity matrix and all-zero vector of size N (omitted when no confusion can occur). $\mathbb{E}[\cdot]$ denotes statistical expectation. $\text{Re}\{\cdot\}$ denotes the real part. The multivariate circularly symmetric complex Gaussian distribution with covariance \mathbf{R} is denoted by $\mathcal{CN}(\mathbf{0}, \mathbf{R})$. \mathbf{D}_x denotes a diagonal matrix with x on its diagonal. \mathbb{R} and \mathbb{C} denote the spaces of real and complex numbers, respectively, and $\mathbb{C}_+ \triangleq \{s \in \mathbb{C} : \text{Re}\{s\} \geq 0\}$ the complex right half-plane. $|\cdot|$, $\|\cdot\|$, and $\|\!\|\!\cdot\!\|$ denote absolute value, vector- or operator norm, and matrix norm, respectively.

II. MOTIVATING EXAMPLE

Before investigating more complex systems, we first consider a simple setup with one BS, one repeater, and two users, as illustrated in Fig. 1. The repeater is placed equidistant from both users. Intuitively, this is an unfavorable scenario, as the users cause strong interference to each other at the repeater.

The direct-link channels (i.e., user-to-BS) are denoted by \mathbf{h}_1 and \mathbf{h}_2 , and the repeater-to-BS (R2B) channel is denoted by \mathbf{g} . All the channels are normalized to have unit gain, i.e., $\|\mathbf{h}_1\| = \|\mathbf{h}_2\| = \|\mathbf{g}\| = 1$, and be mutually orthogonal, i.e., $\mathbf{h}_1^H \mathbf{h}_2 = \mathbf{h}_1^H \mathbf{g} = \mathbf{h}_2^H \mathbf{g} = 0$. The repeater has an amplification gain $\alpha \geq 0$. The received signal at the BS is given by

$$\mathbf{y} = \mathbf{h}_1 x_1 + \mathbf{h}_2 x_2 + \alpha \mathbf{g}(x_1 + x_2) + \mathbf{w}, \quad (1)$$

where x_1 and x_2 represent the signals from the users, and $\mathbf{w} \sim \mathcal{CN}(\mathbf{0}, \zeta^2 \mathbf{I})$ represent the additive white Gaussian noise (AWGN) at the BS.

Since the channels are orthogonal, we can obtain the sufficient statistics for decoding x_1 and x_2 by projecting the received signal \mathbf{y} onto the directions of $\mathbf{h}_1, \mathbf{h}_2, \mathbf{g}$:

$$\begin{cases} \tilde{y}_1 = \mathbf{h}_1^H \mathbf{y} = x_1 + \tilde{w}_1 \\ \tilde{y}_2 = \mathbf{h}_2^H \mathbf{y} = x_2 + \tilde{w}_2 \\ \tilde{y}_3 = \mathbf{g}^H \mathbf{y} = \alpha(x_1 + x_2) + \tilde{w}_3 \end{cases} \quad (2)$$

which can be written as the linear model

$$\tilde{\mathbf{y}} = \underbrace{\begin{bmatrix} \tilde{y}_1 \\ \tilde{y}_2 \\ \tilde{y}_3 \end{bmatrix}}_{\triangleq \mathbf{H}} = \underbrace{\begin{bmatrix} 1 & 0 \\ 0 & 1 \\ \alpha & \alpha \end{bmatrix}}_{\triangleq \mathbf{H}} \begin{bmatrix} x_1 \\ x_2 \end{bmatrix} + \tilde{\mathbf{w}}, \quad (3)$$

where $\mathbf{w} \sim \mathcal{CN}(\mathbf{0}, \varsigma^2 \mathbf{I}_3)$. We consider the best linear unbiased estimator (BLUE) [equivalently, the zero forcing (ZF) combiner] of x_1 and x_2 , given by

$$\begin{bmatrix} \hat{x}_1 \\ \hat{x}_2 \end{bmatrix} = (\mathbf{H}^T \mathbf{H})^{-1} \mathbf{H}^T \tilde{\mathbf{y}}, \quad (4)$$

which has error covariance $\varsigma^2 (\mathbf{H}^T \mathbf{H})^{-1}$; therefore, the variance of each estimate is

$$\frac{1 + \alpha^2}{1 + 2\alpha^2} \varsigma^2 \xrightarrow{\alpha \rightarrow \infty} \frac{1}{2} \varsigma^2. \quad (5)$$

We note that even in this idealized scenario, where channels are orthogonal and the repeater adds no noise, a poorly placed repeater can only offer at most 3 dB signal-to-noise ratio (SNR) gain, at the cost of infinitely large amplification. This limitation is further illustrated in the numerical results shown in Fig. 2, where two users are placed 40 meters apart and 500 meters from the BS. The repeater is moved along a line parallel to, and 40 meters offset from, the line connecting the two users. Both the users and the repeater have a maximum transmit power of 23 dBm, and the repeater amplification gain is constrained to be less than 90 dB. The pathlosses follow the 3GPP models that will be described in Section VI at 6 GHz. The BS uses a minimum mean-square error (MMSE) combiner to decode the users' signals, and the sum rate is obtained by a moving average over the repeater locations for every 4 meters. As we can observe, a repeater placed in the middle of the two users can negatively affect the sum rate due to increased interference. This example illustrates the importance of joint control of the repeater gains and user transmit powers, as well as the need for a systematic analysis of repeater swarm-assisted cellular systems to fully understand the benefits and limitations of deploying swarms of repeaters.

III. SYSTEM MODEL

We consider a single-cell system where an M -antenna BS serves K single-antenna users. To improve coverage, N repeaters are deployed across the cell. The number of BS antennas is more than the number of repeaters, i.e., $M \geq N$, which typically holds in massive MIMO regime.

The repeaters are full-duplex relays with single antenna port, but they can have one or dual physical antennas, as shown in Fig. 3. Type-I repeaters use the same physical antenna for reception and transmission. The received signal is first forwarded to a low-noise amplifier (LNA) and then to a

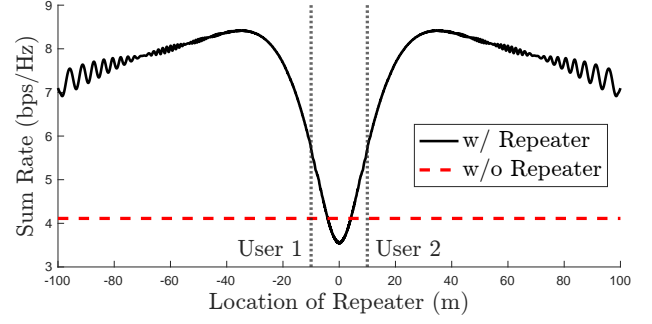


Fig. 2: Averaged sum rate for different repeater locations.

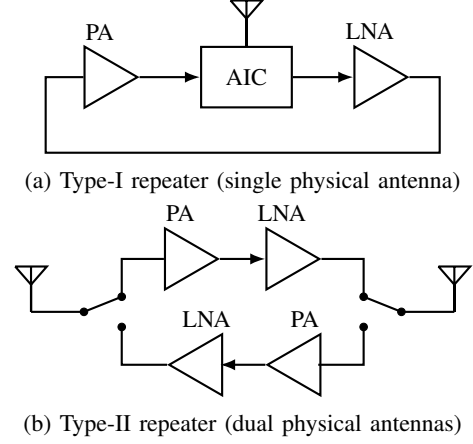


Fig. 3: Block diagrams of repeater (redrawn from [4]).

power amplifier (PA). The self-interference is mitigated by an antenna-interface circuit (AIC), which prevents the amplified signal from the PA to re-enter the LNA. Type-II repeaters employ two physical antennas, one pointing toward the BS and another to the users. A switch is used to select the transmission direction. Compared with type-I repeaters, type-II repeaters can achieve better self-interference cancellation and one antenna can be properly tuned toward the BS for better link quality. However, type-II repeaters must be carefully calibrated for reciprocity-based communication [25].

Each repeater, say repeater n , has the impulse response

$$\mathbf{a}_n(t) = \alpha_n \delta(t - \nu_n), \quad (6)$$

where $\alpha_n \geq 0$ is the *amplification gain*, and $\nu_n > 0$ represents the induced delay. All wireless channels are assumed to be LTI¹ and reciprocal. We use the following notations for the channels of different links (see Fig. 4):²

¹In practice, all wireless channels are time-varying. The assumption of a LTI system, is, strictly speaking, an approximation. However, since the transmission slot is typically much shorter than the channel coherence time, during which the channel response is nearly time-invariant, approximating the system as LTI is reasonable. Analyzing a time-varying system is interesting but much more challenging. We will have to leave it as a future direction.

²These are all passband signals and *not* complex baseband.

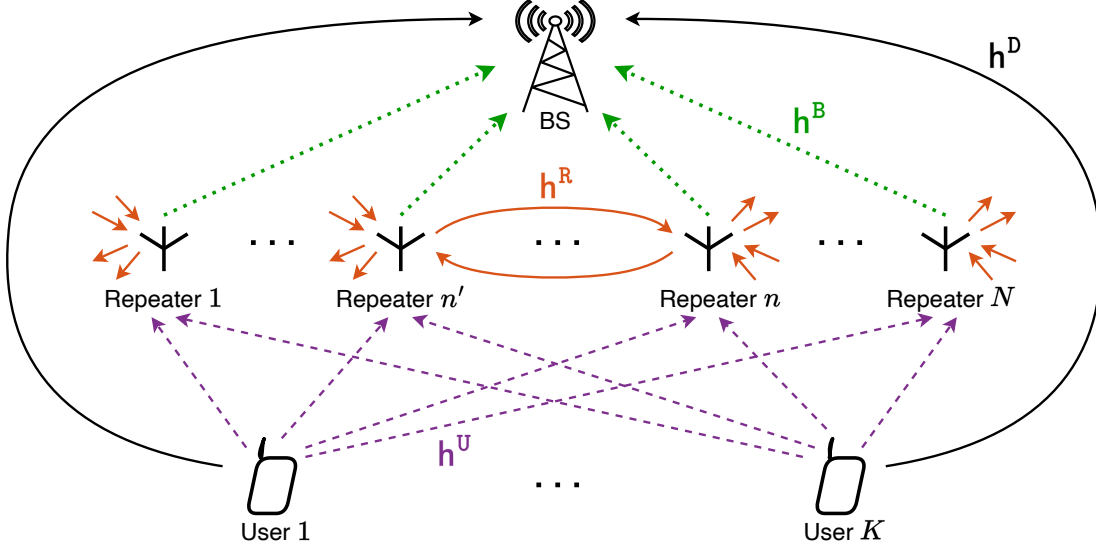


Fig. 4: Illustration of a repeater swarm-assisted cellular system.

$\mathbf{h}_{mk}^D(t)$	D irect Link: user $k \leftrightarrow m$ th BS antenna
$\mathbf{h}_{nk}^U(t)$	U ser-Repeater Link: user $k \leftrightarrow$ repeater n
$\mathbf{h}_{nn'}^R(t)$	R epeater Link: repeater $n \leftrightarrow$ repeater n'
$\mathbf{h}_{mn}^B(t)$	B S-Repeater Link: repeater $n \leftrightarrow m$ th BS antenna

Since we will have to deal with potentially unstable systems, for which the Fourier transform may not exist, we will work in the Laplace domain at this stage. For a function $x(t)$ defined for $t \geq 0$, the Laplace transform is expressed as a function of the complex variable s :

$$x(s) \triangleq \int_0^\infty x(t)e^{-st}dt. \quad (7)$$

For example, the repeater impulse response $a(t)$ in (6) has the following Laplace transform in the region of convergence \mathbb{C}_+ :

$$a_n(s) = \alpha_n e^{-s\nu_n}. \quad (8)$$

The Laplace transforms are written in *Italic font*, $x(s)$, to distinguish the corresponding time functions in *Helvetica font*, $x(t)$. When the Fourier transform exists, we can represent it by choosing $s = j\omega$, where ω is the angular frequency. Once the stability conditions are established in Section IV, we will transition to analysis in the frequency domain.

We next derive the input-output relationship of the repeater swarms, which is used for stability and performance analysis.

A. The Repeater Swarm

The repeaters operate in full-duplex, instantaneously amplifying and retransmitting the received signals. Let $u_n(s)$ denote the input to repeater n , consisting of signals from the intended

sources (i.e., user signals in uplink or BS signal in downlink) and AWGN. The output from repeater n is given by

$$r_n(s) = a_n(s) \left(u_n(s) + \sum_{n'=1}^N h_{nn'}^R(s) r_{n'}(s) \right), \quad (9)$$

where the summand corresponds to the repeater interaction for $n' \neq n$ and self-interference for $n' = n$.

By concatenating (9) for all repeaters, the output from the repeater swarm, $\mathbf{r}(s) \triangleq [r_1(s), \dots, r_N(s)]^T$, satisfies

$$\mathbf{r}(s) = \mathbf{D}_a(s) (\mathbf{u}(s) + \mathbf{H}^R(s) \mathbf{r}(s)), \quad (10)$$

where $\mathbf{a}(s) \triangleq [a_1(s), \dots, a_N(s)]^T$, $\mathbf{u}(s) \triangleq [u_1(s), \dots, u_N(s)]^T$, and

$$\mathbf{H}^R(s) \triangleq \begin{bmatrix} h_{11}^R(s) & \dots & h_{1N}^R(s) \\ \vdots & \ddots & \vdots \\ h_{N1}^R(s) & \dots & h_{NN}^R(s) \end{bmatrix}. \quad (11)$$

We note that $\mathbf{H}^R(s)$ is symmetric due to channel reciprocity; however, it is not Hermitian in general.

By rearranging (10), the input-output relation of the repeater swarm is expressed as

$$\mathbf{r}(s) = \mathbf{G}(s) \mathbf{u}(s), \quad (12)$$

where

$$\mathbf{G}(s) \triangleq (\mathbf{I}_N - \mathbf{D}_a(s) \mathbf{H}^R(s))^{-1} \mathbf{D}_a(s) \quad (13)$$

is the effective transfer function matrix of the repeater swarm. $\mathbf{G}(s)$ corresponds to a multi-dimensional system with a positive feedback loop due to repeater interaction, as illustrated by the block diagram in Fig. 5. Note that $\mathbf{G}(s) = \mathbf{G}(s)^T$ but $\mathbf{G}(s) \neq \mathbf{G}(s)^H$.

We next present the uplink and downlink signal models of the repeater-assisted massive MIMO system.

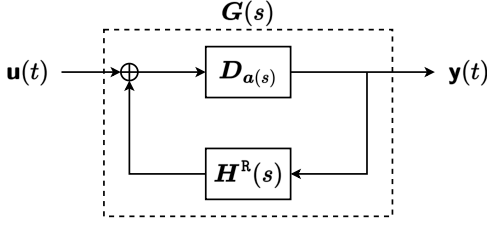


Fig. 5: Block diagram of the positive-feedback system.

B. Uplink Model

Let $x_k^{\text{ul}}(s)$ denote the signal transmitted by user k . Then, the input to the repeater swarm is $\mathbf{u}^{\text{ul}}(s) = \mathbf{H}^{\text{U}}(s)\mathbf{x}^{\text{ul}}(s) + \mathbf{w}^{\text{R,ul}}(s)$, where $\mathbf{x}^{\text{ul}}(s) \triangleq [x_1^{\text{ul}}(s), \dots, x_K^{\text{ul}}(s)]^T$, $\mathbf{H}^{\text{U}}(s) \in \mathbb{C}^{N \times K}$ contains the channel coefficients $\{h_{nk}^{\text{U}}(s)\}$, and $\mathbf{w}^{\text{R,ul}}(s) \in \mathbb{C}^N$ represents the AWGN at the repeaters. The received signal at the BS consists of both the direct-link signals from the users and the signals from the repeaters:

$$\begin{aligned} \mathbf{y}^{\text{ul}}(s) &= \mathbf{H}^{\text{D}}(s)\mathbf{x}^{\text{ul}}(s) + \mathbf{H}^{\text{B}}(s)\mathbf{G}(s)\mathbf{u}^{\text{ul}}(s) + \mathbf{w}^{\text{B}}(s) \\ &= (\mathbf{H}^{\text{D}}(s) + \mathbf{H}^{\text{B}}(s)\mathbf{G}(s)\mathbf{H}^{\text{U}}(s))\mathbf{x}^{\text{ul}}(s) \\ &\quad + \mathbf{H}^{\text{B}}(s)\mathbf{G}(s)\mathbf{w}^{\text{R,ul}}(s) + \mathbf{w}^{\text{B}}(s), \end{aligned} \quad (14)$$

where $\mathbf{H}^{\text{D}}(s) \in \mathbb{C}^{M \times K}$ contains $\{h_{mk}^{\text{D}}(s)\}$, $\mathbf{H}^{\text{B}}(s) \in \mathbb{C}^{M \times N}$ contains $\{h_{mn}^{\text{B}}(s)\}$, and $\mathbf{w}^{\text{B}}(s) \in \mathbb{C}^M$ denotes the AWGN at the BS.

C. Downlink Model

Let $\mathbf{x}^{\text{dl}}(s) \in \mathbb{C}^M$ denote the precoded signal transmitted by the BS. Due to channel reciprocity, the uplink and downlink channel matrices are equal, up to a transpose. Thus, the input to the repeater swarm is $\mathbf{u}^{\text{dl}}(s) = (\mathbf{H}^{\text{B}}(s))^T \mathbf{x}^{\text{dl}}(s) + \mathbf{w}^{\text{R,dl}}(s)$, where $\mathbf{w}^{\text{R,dl}}(s) \in \mathbb{C}^N$ is the repeater noise. The received signal at user k is given by

$$\begin{aligned} y_k^{\text{dl}}(s) &= \mathbf{h}_k^{\text{D}}(s)^T \mathbf{x}^{\text{dl}}(s) + \mathbf{h}_k^{\text{U}}(s)^T \mathbf{G}(s)\mathbf{u}^{\text{dl}}(s) + w_k(s) \\ &= (\mathbf{h}_k^{\text{D}}(s) + \mathbf{H}^{\text{B}}(s)\mathbf{G}(s)\mathbf{h}_k^{\text{U}}(s))^T \mathbf{x}^{\text{dl}}(s) \\ &\quad + (\mathbf{G}(s)\mathbf{h}_k^{\text{U}}(s))^T \mathbf{w}^{\text{R,dl}}(s) + w_k(s), \end{aligned} \quad (15)$$

where $\mathbf{h}_k^{\text{D}}(s)$ and $\mathbf{h}_k^{\text{U}}(s)$ denote the k th columns of $\mathbf{H}^{\text{D}}(s)$ and $\mathbf{H}^{\text{U}}(s)$, respectively, and w_k represents the AWGN at user k .

IV. STABILITY ANALYSIS

Repeater interactions create a positive feedback loop, requiring careful configuration to prevent instability. Stability of the system is fully determined by the *joint* response of the repeater swarm and is *agnostic* to whether the system operates in the uplink or downlink. In this section, we investigate the conditions for system stability.

A. Bounded-Energy Stability

Before it becomes relevant to analyze stability of the system, it is necessary to first verify that the system is well-defined—specifically, that the transfer function matrix $\mathbf{G}(s)$ represents the Laplace transform of a *unique* and *causal* impulse response $\mathbf{G}(t)$. We will formally address this point in Theorem 1. For now, assuming the system is well-defined and $\mathbf{G}(t)$ exists, we

introduce the bounded-energy stability criterion. The relevant definitions are given as follows.

Definition 1. A time signal $\mathbf{u}(t)$ of arbitrary dimension is said to have finite energy if $\int_{-\infty}^{+\infty} \mathbf{u}(t)^T \mathbf{u}(t) dt < \infty$.

Definition 2. An LTI system with a causal impulse response $\mathbf{G}(t)$ of arbitrary dimension is bounded energy stable if, for any input signal $\mathbf{u}(t)$ with finite energy, the output signal $\int_0^t \mathbf{G}(\tau)\mathbf{u}(t-\tau)d\tau$ has finite energy.

Remark 1. Bounded-energy stability ensures that the system remains stable for bounded-energy inputs. The system is bounded-energy stable if its transfer function has a finite \mathcal{H}_{∞} norm [26, Th. 4.3].

Remark 2. Although stability has been extensively studied in control theory, most existing results are derived under the assumption that the system has a rational transfer function; see, for example, the Nyquist stability criterion in [27, Th. 4.7]. The presence of time delays—which are inherent in communication systems—results in infinite-dimensional state spaces that do not have a rational transfer function. While it is generally true that the Nyquist stability criterion applies to non-rational systems as well, a rigorous proof of this fact is involved; see, for instance, [28]. (In [28], bounded-input bounded-output stability is considered only for one-dimensional systems, rather than the bounded-energy stability for multi-dimensional systems we consider here.)

To establish our main results on stability, we introduce the following two assumptions.

Assumption 1. The transfer function matrix $\mathbf{H}^{\text{R}}(s)$ is analytic in the right half-plane \mathbb{C}_+ .³

Assumption 2. There exist constants $C, \varepsilon, \delta > 0$ such that the inter-repeater channel amplitude gain satisfies $|h_{nn'}^{\text{R}}(s)| \leq \frac{C}{|s|^{1+\varepsilon}}$ for all $|s| \geq \delta$ in \mathbb{C}_+ for all $n, n' \in \{1, 2, \dots, N\}$.

Remark 3. Physically, Assumption 2 implies that the channel amplitude decays with frequency at a rate faster than $1/|s|$ for large $|s|$. This reflects practical wireless propagation behavior: in free space, the channel amplitude already scales as $1/|\omega|$ due to the decreasing effective aperture of antennas, and in real environments, due to lossy media or material penetration, the attenuation is even faster. Additionally, antennas and RF front-ends inherently act as bandpass filters, limiting the response at high frequencies.

We now give our main results in the following theorem.

Theorem 1. Under Assumptions 1 and 2, if the image of $\det(\mathbf{I}_N - \mathbf{D}_a(j\omega)\mathbf{H}^{\text{R}}(j\omega))$ does not encircle the origin, then for $\mathbf{G}(s)$ defined in (13), the impulse response

$$\mathbf{G}(t) \triangleq \frac{1}{j2\pi} \int_{\sigma-j\infty}^{\sigma+j\infty} \mathbf{G}(s)e^{st} ds \quad (16)$$

exists for all $\sigma \geq 0$ and is independent of the choice of σ . Additionally, $\mathbf{G}(t)$ is causal, i.e., $\mathbf{G}(t) = \mathbf{0}$ for $t < 0$, and bounded-energy stable.

³Strictly speaking, a function is considered analytic only in open sets. Therefore, when we say a function is analytic in \mathbb{C}_+ , we mean there exists a $\gamma > 0$ such that the function is analytic in $\{s \in \mathbb{C} : \text{Re}(s) > -\gamma\}$.

Proof: See Appendix. ■

Remark 4. When the conditions in Theorem 1 holds, the region of convergence of the Laplace transform includes the $j\omega$ axis; hence, the Fourier transform $\mathbf{G}(j\omega)$ is well-defined, allowing us to analyze the system in the frequency domain.

Remark 5. Theorem 1 generalizes the Nyquist stability criterion in [27, Th. 4.7] to the particular multi-dimensional system that we study in this paper.

B. Simplified Condition for Interaction Stability

Theorem 1 provides a stability condition expressed in terms of the image of the complex-valued function $\det(\mathbf{I}_N - \mathbf{D}_{\mathbf{a}(j\omega)} \mathbf{H}^R(j\omega))$. This function has a complicated appearance in general (see example in Fig. 7a), making the result difficult to apply in practice. To guide practical system design, we develop a *sufficient*, more restrictive, condition for stability, which is much simpler and depends explicitly on the channel gains between repeaters. The key idea is to apply Gershgorin disc theorem to find the region, i.e., union of discs, where the eigenvalues of $\mathbf{I}_N - \mathbf{D}_{\mathbf{a}(j\omega)} \mathbf{H}^R(j\omega)$ are located and make sure they are bounded away from zero.

Proposition 1. *The non-encirclement condition in Theorem 1 is satisfied if $\sup_{\omega \in \mathbb{R}} D(\alpha; \omega) < 1$, where*

$$D(\alpha; \omega) \triangleq \min \{D_1(\alpha; \omega), D_2(\alpha; \omega)\}, \quad (17)$$

with

$$D_1(\alpha; \omega) \triangleq \max_n \alpha_n \sum_{n'=1}^N |h_{nn'}^R(j\omega)|, \quad (18a)$$

$$D_2(\alpha; \omega) \triangleq \max_n \sum_{n'=1}^N \alpha_{n'} |h_{nn'}^R(j\omega)|. \quad (18b)$$

Proof: By applying the Gershgorin disc theorem [29, Th. 6.1.1] to both the rows and columns of $\mathbf{D}_{\mathbf{a}(j\omega)} \mathbf{H}^R(j\omega)$, it follows that for an arbitrary ω , all eigenvalues of $\mathbf{D}_{\mathbf{a}(j\omega)} \mathbf{H}^R(j\omega)$ lie within the intersection of the Gershgorin sets:

$$\bigcup_n \left\{ z \in \mathbb{C} : |z - a_n h_{nn}^R(j\omega)| \leq \alpha_n \sum_{n' \neq n} |h_{nn'}^R(j\omega)| \right\},$$

$$\bigcup_n \left\{ z \in \mathbb{C} : |z - a_n h_{nn}^R(j\omega)| \leq \sum_{n' \neq n} \alpha_{n'} |h_{nn'}^R(j\omega)| \right\},$$

which are enclosed by the circles centered at the origin with radii $D_1(\alpha; \omega)$ and $D_2(\alpha; \omega)$, respectively. Therefore, their intersection lies within the circle centered at the origin with radius $D(\alpha; \omega)$. (The use of Gershgorin disc theorem in relation to multivariable Nyquist techniques was also exploited in, for example, [30, Ch. 2.10].)

To proceed, notice that $D(\alpha; \omega)$ is a monotonically non-decreasing function of α , i.e., $D(\alpha'; \omega) \geq D(\alpha; \omega)$ for any α' such that $\alpha'_n \geq \alpha_n, \forall n$. When all repeaters are turned off, i.e., $\alpha_n = 0$, the image of $\det(\mathbf{I}_N - \mathbf{D}_{\mathbf{a}(j\omega)} \mathbf{H}^R(j\omega))$ collapses to a single point at $1 + j0$, and the system is trivially stable. As the amplification gains continuously increase from zero, the image of $\det(\mathbf{I}_N - \mathbf{D}_{\mathbf{a}(j\omega)} \mathbf{H}^R(j\omega))$ will continuously change,

and the system will remain stable as long as the image has not yet intersected the origin. The non-intersection of that image with the origin can be guaranteed if $D(\alpha; \omega) < 1$ for all ω . ■

Remark 6. While checking the conditions for Proposition 1 requires evaluating the inter-repeater channel gains for all frequencies, this can be simplified in practice. Since wireless systems operate within a limited frequency range and antennas inherently function as bandpass filters, it is generally sufficient to verify the condition within the operational frequency range of interest (e.g., 20 MHz bandwidth at 6 GHz and 100 MHz at 30 GHz, 60 GHz, and 70 GHz [31, Table 7.8-2]). Alternatively, one could get a looser bound by taking the maximum over ω for each $h_{nn'}^R(j\omega)$ term inside the expression of $D(\alpha; \omega)$ —for each inter-repeater link, we only need to know the maximum channel gain over the operating frequency band. Nevertheless, it is worth noting that spurious emissions, amplifier harmonics, and wideband interference or jamming may introduce out-of-band behavior that could, in some cases, affect the system. A wider-spectrum analysis could offer further insights in scenarios where such effects become non-negligible.

C. Special Cases

To gain further insights, we consider the special case where all repeaters have the same amplification gain α .

Corollary 1. *For the special case when $a_n(s) = \alpha e^{-s\nu_n}, \forall n$, the non-encirclement condition in Theorem 1 is satisfied if*

$$\alpha < \alpha_G \triangleq \inf_{\omega} \min_n \frac{1}{\sum_{n'=1}^N |h_{nn'}^R(j\omega)|}. \quad (20)$$

Remark 7. Corollary 1 was presented in [1] when ignoring the time-delay.⁴ The Gershgorin theorem analysis is the same but [1] postulated without proof that stability holds if $\mathbf{I} - \alpha' \mathbf{H}^R(j\omega)$ is non-singular for all ω and $\alpha' \leq \alpha$; we prove this rigorously here.

Remark 8. For stability of the repeater swarm, it is the sum of channel *amplitude* gains that matters, rather than the sum of channel *power* gains. In the worst case, the positive feedback combines constructively, in-phase, behaving as if the repeaters formed a coherent antenna array.

Next, we consider two examples with line-of-sight (LoS) channels and ignore the channel gain variation with frequency (narrow enough bandwidth of the signal), such that

$$h_{nn'}^R(s) = \sqrt{\beta_{nn'}^R} e^{-s\tau_{nn'}}, \quad (21)$$

where $\beta_{nn'}^R$ is the channel power gain and $\tau_{nn'}$ is the propagation delay that are both determined by the distance $d_{nn'}$. The condition in Corollary 1 simplifies to

$$\alpha < \alpha_G = \min_n \frac{1}{\sum_{n' \neq n} \sqrt{\beta_{nn'}^R}}. \quad (22)$$

For simplicity, we also consider that all repeaters have the same delay ν , such that $a_n(s) = a(s) = \alpha e^{-s\nu}, \forall n$.

⁴In [1] it was erroneously mentioned in the concluding remarks that as a possible extension of the analysis, α could be complex-valued. But it cannot be since α applies to the passband signal. What was intended by that remark in [1] is that a time-delay of the repeater could be included in the model, which we have done herein.

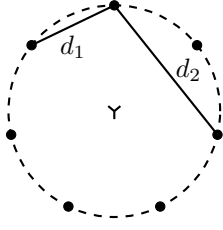


Fig. 6: Repeaters equally spaced on a circle.

1) *Two Repeaters*: Consider the case of $N = 2$ repeaters. We can write for simplicity $h_{12}(s) = h_{21}(s) = \sqrt{\beta}e^{-s\tau}$, and the inter-repeater channel transfer function matrix is

$$\mathbf{H}^R(s) = \begin{bmatrix} 0 & \sqrt{\beta}e^{-s\tau} \\ \sqrt{\beta}e^{-s\tau} & 0 \end{bmatrix}; \quad (23)$$

therefore,

$$\det(\mathbf{I}_2 - a(s)\mathbf{H}^R(s)) = 1 - \alpha^2\beta e^{-2s(\tau+\nu)}. \quad (24)$$

The image of $\det(\mathbf{I}_2 - a(j\omega)\mathbf{H}^R(j\omega))$ traces out a circle centered at $1 + j0$ with radius $\alpha^2\beta$ anticlockwise and periodically for every change of ω by $\pi/(\tau+\nu)$. According to Theorem 1, the system is stable if $\alpha^2\beta < 1$.

For this particular case, the following recursive equations can be written in the time domain:

$$r_1(t) = \alpha u_1(t - \nu) + \alpha\sqrt{\beta} r_2(t - \tau - \nu), \quad (25a)$$

$$r_2(t) = \alpha u_2(t - \nu) + \alpha\sqrt{\beta} r_1(t - \tau - \nu), \quad (25b)$$

which yield the output of the two repeaters as

$$r_1(t) = \alpha u_1(t - \nu) * p(t) + \alpha^2\sqrt{\beta} u_2(t - \nu) * p(t - \tau - \nu),$$

$$r_2(t) = \alpha u_2(t - \nu) * p(t) + \alpha^2\sqrt{\beta} u_1(t - \nu) * p(t - \tau - \nu).$$

Here, $p(t)$ represents the impulse train

$$p(t) = \sum_{i=0}^{\infty} (\alpha^2\beta)^i \delta(t - 2i(\tau + \nu)), \quad (27)$$

which represents the “ping-pong” effect of the loopback signal between the two repeaters. The system is stable if $\alpha^2\beta < 1$, ensuring that the impulse train decays exponentially to zero. It is noteworthy that both Theorem 1 and Proposition 1 provide necessary and sufficient conditions for this special case.

2) *Repeaters on Circle*: Consider an odd number of repeaters, $N = 2N_0 + 1$, for some integer N_0 , uniformly spread over a circle with radius R . (The analysis carries over to an even number of repeaters with slight changes, omitted here for brevity.) Next, with a slight abuse of notation, we define

$$d_i \triangleq 2R \sin(i\pi/N), \quad (28)$$

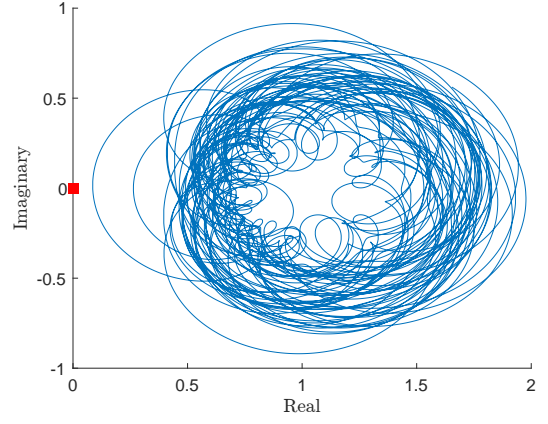
and denote the channel power gain and the delay at distance d_i as β_i and τ_i , respectively. By indexing the repeaters in the clockwise order, the channel between repeaters n and n' is

$$h_i^R(s) \triangleq \sqrt{\beta_i} e^{-s\tau_i}, \quad (29)$$

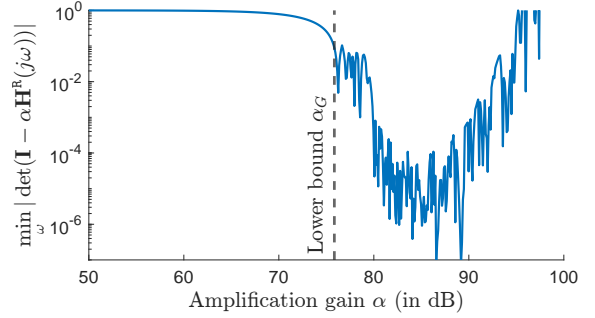
with

$$i = \min\{|n - n'|, N - |n - n'|\}. \quad (30)$$

See Fig. 6 for a graphical illustration.



(a) The image of $\det(\mathbf{I}_N - \alpha\mathbf{H}^R(j\omega))$ with the amplification gain $\alpha = \alpha_G \approx 75.8$ dB



(b) Plot of $\min_{\omega} |\det(\mathbf{I}_N - \alpha\mathbf{H}^R(j\omega))|$ for different α

Fig. 7: Numerical results when 15 repeaters are uniformly spaced on a circle with a radius of 1000 meters.

In this particular case, $\mathbf{H}^R(s)$ is symmetric circulant with each column being a circulant permutation of the vector

$$\mathbf{q}(s) \triangleq [0, h_1^R(s), \dots, h_{N_0}^R(s), h_{N_0}^R(s), \dots, h_1^R(s)]^T. \quad (31)$$

We can now compute all eigenvalues of $\mathbf{H}^R(j\omega)$ as the discrete Fourier transform (DFT) of $\mathbf{q}(j\omega)$, and obtain

$$\det(\mathbf{I}_N - a(j\omega)\mathbf{H}^R(j\omega)) = \prod_{n=1}^N \left(1 - 2\alpha \sum_{i=1}^{N_0} \left(\sqrt{\beta_i} \cos \frac{2\pi i(n-1)}{N} \right) e^{-j\omega(\tau_i + \nu)} \right). \quad (32)$$

Although (32) provides a closed-form expression, determining the shape of the image of $\det(\mathbf{I} - a(j\omega)\mathbf{H}^R(j\omega))$ and whether it encircles the origin for an arbitrary α remains challenging.

We visualize the image of $\det(\mathbf{I} - \alpha\mathbf{H}^R(j\omega))$ in Fig. 7a under the free-space propagation model $\beta_i = c^2/(2\omega d_i)^2$ and $\tau_i = d_i/c$. The repeater amplification gains are selected as the critical value α_G , which guarantees interaction stability according to Corollary 1. The samples are taken by frequency sweeping over a 20 MHz band centered at 2 GHz, with a step size of 100 Hz. Notice that even in this special case, appearance of the image is quite complex. Additionally, in Fig. 7b, we plot the minimum value of $|\det(\mathbf{I}_N - \alpha\mathbf{H}^R(j\omega))|$ over the sampled frequency points for different values of α . It can be observed that the critical value α_G accurately captures the transition point at which the system starts to become unstable.

D. How much of the instability effect will be seen within a coherence time interval?

For a finite-dimensional causal system with a proper rational transfer function, the stability is determined by the poles of the transfer function. If all poles are in the left half-plane (therefore have negative real parts), the system is stable; after triggered by an impulse, the system response will converge to a zero after a transient time. The order of magnitude of the transient time is determined by the pole closest to the imaginary axis, say p , which corresponds to an output that exponentially decays with the rate $e^{-|\operatorname{Re}(p)|t}$.

For an unstable system of finite dimension, one can make a rational fraction expansion of the transfer function. The term with the pole furthest into the right half plane will eventually dominate over the other terms, and determines the instability behavior as t grows.

However, since we have a system with time-delays, it has infinite dimension and does not have a rational transfer function. Hence, the argument above does not directly apply. We have to leave a more accurate, quantitative investigation of the instability behavior for future work.

V. UPLINK PERFORMANCE

In this section, we analyze the communication performance of the repeater-assisted system. All the analyses are performed in the frequency domain, within the coherence bandwidth centered at an arbitrary carrier (angular) frequency ω . Hence, the received signal follows the uplink model in (14) and the downlink model in (15), with $s = j\omega$. For brevity, we focus on the uplink; once the uplink performance is determined, one can analyze or optimize the downlink by exploiting uplink-downlink duality [32]. We also note that, as observed in [15], uplink communications benefit more from repeaters due to the limited transmit power of user devices.

Remark 9. We consider a single-carrier, narrowband system for ease of exposition. However, all results can be extended to multi-carrier (wideband) systems. In principle, the optimization for a multi-carrier system has the same problem structure as (P1) presented below—it introduces an outer sum over the sub-carriers in the objective function, and the same solution techniques can be applied. The optimization variables (combining vectors, repeater gains, and user powers) can either be kept the same for all sub-carriers or optimized independently for each sub-carrier.

We first rewrite the received signal in (14) as

$$\mathbf{y}(j\omega) = \mathbf{H}(j\omega)\mathbf{x}(j\omega) + \mathbf{w}(j\omega), \quad (33)$$

where the composite uplink channel, $\mathbf{H}(j\omega)$, and aggregate noise at the BS, $\mathbf{w}(j\omega)$, are respectively expressed as

$$\mathbf{H}(j\omega) \triangleq \mathbf{H}^D(j\omega) + \mathbf{H}^B(j\omega)\mathbf{G}(j\omega)\mathbf{H}^U(j\omega), \quad (34a)$$

$$\mathbf{w}(j\omega) \triangleq \mathbf{w}^B(j\omega) + \mathbf{H}^B(j\omega)\mathbf{G}(j\omega)\mathbf{w}^R(j\omega). \quad (34b)$$

With this model, we first analyze the uplink capacity and then develop a linear combining scheme to maximize the weighted sum rate through joint repeater gain configuration and user power control under the interaction stability constraint.

For clarity, the explicit dependence on $j\omega$ and the superscript $(\cdot)^{\text{ul}}$ will be omitted henceforth. It is worth noting that performance metrics such as capacity, signal-to-interference-plus-noise ratio (SINR), and achievable rates may, in general, vary with frequency.

A. Capacity Analysis

Let $\mathbf{w}^B \sim \mathcal{CN}(\mathbf{0}, \varsigma_B^2 \mathbf{I}_M)$ and $\mathbf{w}^R \sim \mathcal{CN}(\mathbf{0}, \varsigma_R^2 \mathbf{I}_N)$, where ς_B^2 and ς_R^2 are the noise powers at the BS and repeaters, respectively. The aggregate noise \mathbf{w} is therefore colored Gaussian, i.e., $\mathbf{w} \sim \mathcal{CN}(\mathbf{0}, \boldsymbol{\Sigma})$, with covariance matrix

$$\boldsymbol{\Sigma} = \varsigma_B^2 \mathbf{I}_M + \varsigma_R^2 \mathbf{H}^B \mathbf{G} \mathbf{G}^H (\mathbf{H}^B)^H. \quad (35)$$

We can pre-whiten the received signal as

$$\boldsymbol{\Sigma}^{-\frac{1}{2}} \mathbf{y} = \boldsymbol{\Sigma}^{-\frac{1}{2}} \mathbf{H} \mathbf{x} + \boldsymbol{\Sigma}^{-\frac{1}{2}} \mathbf{w}, \quad (36)$$

where $\boldsymbol{\Sigma}^{-\frac{1}{2}} \mathbf{w} \sim \mathcal{CN}(\mathbf{0}, \mathbf{I}_M)$.

The pre-whitened signal model in (36) represents a MIMO multiple-access channel with AWGN. Considering the power constraint $\mathbb{E}[|x_k|^2] \leq P_{\max}$ for each user, the sum capacity of the system is given by [33]

$$\begin{aligned} C_{\text{sum}} &= \log \det \left(\mathbf{I}_M + P_{\max} \boldsymbol{\Sigma}^{-\frac{1}{2}} \mathbf{H} \mathbf{H}^H \boldsymbol{\Sigma}^{-\frac{1}{2}} \right) \\ &= \log \det \left(\mathbf{I}_M + P_{\max} \boldsymbol{\Sigma}^{-1} \mathbf{H} \mathbf{H}^H \right). \end{aligned} \quad (37)$$

Let $\{R_k\}_{k=1}^K$ denote the achievable rates of all users. The uplink capacity region of the system can be expressed as [33]

$$\begin{aligned} &\left\{ (R_1, \dots, R_K) : \forall \mathcal{S} \subset \{1, 2, \dots, K\}, \right. \\ &\quad \left. \sum_{k \in \mathcal{S}} R_k \leq \log \det \left(\mathbf{I}_M + P_{\max} \boldsymbol{\Sigma}^{-1} \sum_{k \in \mathcal{S}} \mathbf{h}_k \mathbf{h}_k^H \right) \right\}, \end{aligned} \quad (38)$$

where \mathbf{h}_k denotes the k th column of \mathbf{H} .

B. Linear Combining & Weighted Sum-Rate Maximization

Achieving the sum capacity in (37) requires the use of successive interference cancellation (SIC), which is nonlinear and computationally difficult in practice. We instead consider linear combining—the BS uses a vector $\mathbf{c}_k \in \mathbb{C}^M$ to combine the received signal so as to decode data from user k . The signal after combining is

$$\begin{aligned} \hat{q}_k &\triangleq \mathbf{c}_k^H \mathbf{y} = \mathbf{c}_k^H \mathbf{H} \mathbf{x} + \mathbf{c}_k^H \mathbf{w} \\ &= \sqrt{\rho_k} \mathbf{c}_k^H \mathbf{h}_k q_k + \underbrace{\sum_{k' \neq k} \sqrt{\rho_{k'}} \mathbf{c}_k^H \mathbf{h}_{k'} q_{k'} + \mathbf{c}_k^H \mathbf{w}}_{\text{interference-plus-noise}}, \end{aligned} \quad (39)$$

where we express the transmit signal as $x_n \triangleq \sqrt{\rho_k} q_k$; here, q_k is the data symbol of user k with $\mathbb{E}[|q_k|^2] = 1$, and $\rho_k \in [0, P_{\max}]$ denotes the transmit power.

Considering uncorrelated data symbols, the instantaneous SINR of user k is

$$\text{SINR}_k = \frac{\rho_k \mathbf{c}_k^H \mathbf{h}_k \mathbf{h}_k^H \mathbf{c}_k}{\mathbf{c}_k^H \left(\sum_{k' \neq k} \rho_{k'} \mathbf{h}_{k'} \mathbf{h}_{k'}^H + \boldsymbol{\Sigma} \right) \mathbf{c}_k}, \quad (40)$$

which is a generalized Rayleigh quotient with respect to \mathbf{c}_k , and can be maximized by choosing MMSE combiner⁵

$$\mathbf{c}_k^{\text{mmse}} = \sqrt{\rho_k} (\mathbf{H} \mathbf{D}_\rho \mathbf{H}^H + \mathbf{\Sigma})^{-1} \mathbf{h}_k. \quad (41)$$

The resulting SINR with the MMSE combiner becomes

$$\begin{aligned} \text{SINR}_k^{\text{mmse}} &= \rho_k \mathbf{h}_k^H \left(\sum_{k' \neq k} \rho_{k'} \mathbf{h}_{k'} \mathbf{h}_{k'}^H + \mathbf{\Sigma} \right)^{-1} \mathbf{h}_k \\ &= \frac{1}{1 - \rho_k \mathbf{h}_k^H (\mathbf{H} \mathbf{D}_\rho \mathbf{H}^H + \mathbf{\Sigma})^{-1} \mathbf{h}_k} - 1, \end{aligned} \quad (42)$$

where the equality follows from [34, Lemma B.4].

Now, the weighted sum-rate maximization problem under the repeater stability constraint can be formulated as

$$\begin{aligned} \text{maximize}_{\{\mathbf{c}_k\}, \boldsymbol{\rho}, \boldsymbol{\alpha}} \quad & \sum_{k=1}^K \gamma_k \log(1 + \text{SINR}_k) \end{aligned} \quad (\text{P1})$$

$$\text{s.t.} \quad 0 \leq \rho_k \leq P_{\max}, \quad \forall k \quad (\text{C1})$$

$$0 \leq \alpha_n \leq A_{\max}, \quad \forall n \quad (\text{C2})$$

$$\begin{cases} \alpha_n \sum_{n'=1}^N |h_{nn'}^R| \leq \eta, \quad \forall n, \text{ or} \\ \sum_{n'=1}^N \alpha_{n'} |h_{nn'}^R| \leq \eta, \quad \forall n \end{cases} \quad (\text{C3})$$

where $\boldsymbol{\rho}$ and $\boldsymbol{\alpha}$ denote the collections of all $\{\rho_k\}$ and $\{\alpha_n\}$, respectively, $\gamma_k \geq 0$ is the weight that represents the priority of user k , A_{\max} is the maximum amplification gain of repeaters, and $\eta \in (0, 1]$ is a pre-determined parameter that ensures that the repeaters operate away from the instability boundary (additionally, η can provide a margin for robust stability under channel uncertainties). Constraint (C3) is derived from the interaction stability requirements in Corollary 1. Notice that either one of the conditions in (C3) is sufficient for stability according to Proposition 1, and they are both linear constraints.

Simplification $\mathbf{G} = \mathbf{D}_a$: The repeater frequency responses, \mathbf{a} , are absorbed—in a complicated way—in the matrix $\mathbf{G} = (\mathbf{I} - \mathbf{D}_a \mathbf{H}^R)^{-1} \mathbf{D}_a$, which appears in the composite channel matrix \mathbf{H} and the noise covariance $\mathbf{\Sigma}$. For tractability, we ignore the inter-repeater interaction and consider $\mathbf{G} = \mathbf{D}_a$ when solving the optimization problem. This simplification may lead to sub-optimality, as the model adopted for optimization is mismatched from the true model. However, by imposing the stability constraint (C3), the inter-repeater interaction should be kept small, making $\mathbf{G} \approx \mathbf{D}_a$ a reasonable approximation for balancing complexity against performance.

Remark 10. The repeaters add time-delays $\{\nu_n\}$, which, as shown in (8), introduce *frequency-dependent* phase shifts $\{e^{-j\omega\nu_n}\}$ in the frequency responses. While all of our analyses account for arbitrary phase shifts, we restrict the optimization to the real-valued amplification gains α . In principle, it is possible for the repeaters to actively adjust time-delays to control the phase shifts $\{e^{-j\omega\nu_n}\}$, so that the signals from

different repeaters can combine more constructively at the BS for a specific frequency ω . However, this would significantly complicate the optimization problem, increase the operational complexity of the repeaters, and make the system more sensitive to instantaneous channel variations. Such complexity is undesirable, as the repeaters are intended to be simple, low-cost devices that require infrequent reconfiguration to maintain maximum transparency to the network. We will leave the optimization of time-delays for possible future work.

The objective function of (P1) is non-convex, making it difficult to solve. To circumvent this problem, we use the fact that the weighted sum-rate maximization problem has the same optimal solution as a weighted MMSE problem [35, Th. 1]. To see this, we first write the MSE of user k as

$$\begin{aligned} \xi_k &\triangleq \mathbb{E} [|\hat{q}_k - q_k|^2] \\ &= \mathbf{c}_k^H (\mathbf{H} \mathbf{D}_\rho \mathbf{H}^H + \mathbf{\Sigma}) \mathbf{c}_k - 2\sqrt{\rho_k} \text{Re} \{ \mathbf{c}_k^H \mathbf{h}_k \} + 1. \end{aligned} \quad (43)$$

The weighted MMSE problem is then formulated as

$$\begin{aligned} \text{minimize}_{\boldsymbol{\varpi}, \{\mathbf{c}_k\}, \boldsymbol{\rho}, \boldsymbol{\alpha}} \quad & \sum_{k=1}^K \gamma_k (\varpi_k \xi_k - \log \varpi_k) \end{aligned} \quad (\text{P2})$$

$$\text{s.t.} \quad (\text{C1}), (\text{C2}), (\text{C3}),$$

$$\varpi_k \geq 0, \quad \forall k, \quad (\text{C4})$$

where a new variable $\boldsymbol{\varpi} = [\varpi_1, \dots, \varpi_K]^T$ is introduced to represent the MSE weights. Optimizing $\boldsymbol{\varpi}$ when fixing $\boldsymbol{\rho}$, $\boldsymbol{\alpha}$, and $\{\mathbf{c}_k\}$ gives $\varpi_k^{\text{opt}} = 1/\xi_k$. After substituting ϖ_k^{opt} back, the new optimization objective (after removing irrelevant constant terms) is to minimize $\sum_{k=1}^K \gamma_k \log \xi_k$, and the optimal $\{\mathbf{c}_k\}$ when fixing $\boldsymbol{\rho}$ and $\boldsymbol{\alpha}$ are the MMSE combiners in (41). Upon substituting $\{\mathbf{c}_k^{\text{mmse}}\}$, the optimization objective becomes minimizing $\sum_{k=1}^K \gamma_k \log \xi_k^{\text{mmse}}$, where

$$\begin{aligned} \xi_k^{\text{mmse}} &= 1 - \rho_k \mathbf{h}_k^H (\mathbf{H} \mathbf{D}_\rho \mathbf{H}^H + \mathbf{\Sigma})^{-1} \mathbf{h}_k \\ &= 1 - \sqrt{\rho_k} \mathbf{h}_k^H \mathbf{c}_k^{\text{mmse}}. \end{aligned} \quad (44)$$

Comparing with (42), one can observe $\log \xi_k^{\text{mmse}} = -\log(1 + \text{SINR}_k^{\text{mmse}})$. Clearly, (P1) and (P2) are equivalent and have the same optimal solution for $\{\mathbf{c}_k\}$, $\boldsymbol{\rho}$ and $\boldsymbol{\alpha}$.

To solve the weighted MMSE problem in (P2), we adopt a block coordinate descent algorithm similar to the one proposed in [35], where we sequentially optimize one of the variables $\boldsymbol{\varpi}, \{\mathbf{c}_k\}, \boldsymbol{\rho}, \boldsymbol{\alpha}$ while keeping the others fixed; as we will show, each sub-problem is convex. As discussed above, the optimal $\boldsymbol{\varpi}$ is given by $\varpi_k^{\text{opt}} = 1/\xi_k^{\text{mmse}}, \forall k$, where ξ_k^{mmse} is given in (44), and the optimal $\{\mathbf{c}_k\}$ are the MMSE combiners in (41). We next derive the update rule for $\boldsymbol{\rho}$ and $\boldsymbol{\alpha}$.

Update Rule for $\boldsymbol{\rho}$: After substituting (43) into (P2) and omitting terms that do not depend on $\boldsymbol{\rho}$, we can rewrite the objective function as⁶

$$\begin{aligned} & \sum_{k=1}^K \gamma_k \varpi_k \left(\sum_{k'=1}^K \rho_{k'} |\mathbf{c}_{k'}^H \mathbf{h}_{k'}|^2 - 2\sqrt{\rho_k} \text{Re} \{ \mathbf{c}_k^H \mathbf{h}_k \} \right) \\ &= \sum_{k=1}^K \left(\rho_k \sum_{k'=1}^K \gamma_{k'} \varpi_{k'} |\mathbf{c}_{k'}^H \mathbf{h}_{k'}|^2 - 2\sqrt{\rho_k} \gamma_k \varpi_k \text{Re} \{ \mathbf{c}_k^H \mathbf{h}_k \} \right), \end{aligned}$$

⁵Notice that the scaling factor is canceled out in the ratio and is therefore irrelevant for SINR or rate maximization. We chose the particular scaling because it also minimizes the mean-square error (MSE).

⁶Notice that, when choosing \mathbf{c}_k as the MMSE combiner in (41), $\mathbf{c}_k^H \mathbf{h}_k$ is positive-valued; thus, the $\text{Re}\{\cdot\}$ operation can be omitted.

which, along with the power constraint (C1), decouples across users for different ρ_k . The optimization of ρ can thus be solved independently for each user k as

$$\begin{aligned} \min_{\rho_k} \quad & \sum_{k'=1}^K \gamma_{k'} \varpi_{k'} |c_{k'}^H \mathbf{h}_k|^2 - 2\sqrt{\rho_k} \gamma_k \varpi_k \operatorname{Re}\{c_k^H \mathbf{h}_k\} \quad (\text{S1}) \\ \text{s.t.} \quad & 0 \leq \rho_k \leq P_{\max} \end{aligned}$$

The objective function of (S1) is a one-dimensional quadratic function of $\sqrt{\rho_k}$, and the optimal solution is given by

$$\rho_k^{\text{opt}} = \min \left\{ P_{\max}, \left(\frac{\gamma_k \varpi_k \operatorname{Re}\{c_k^H \mathbf{h}_k\}}{\sum_{k'=1}^K \gamma_{k'} \varpi_{k'} |c_{k'}^H \mathbf{h}_k|^2} \right)^2 \right\}. \quad (45)$$

Update Rule for α : Since we are only interested in optimizing the real-valued amplification gains α , we can absorb the phase shifts into the BS-repeater channels by defining $\tilde{\mathbf{H}}^B$, whose columns are obtained by phase-shifting the corresponding columns in \mathbf{H}^B , i.e., $\tilde{\mathbf{h}}_n^B \triangleq e^{j\omega \nu_n} \mathbf{h}_n^B$. After the above simplification, we have $\mathbf{H} = \mathbf{H}^D + \tilde{\mathbf{H}}^B \mathbf{D}_\alpha \mathbf{H}^U$ and $\Sigma = \mathbf{I} + \zeta^2 \tilde{\mathbf{H}}^B \mathbf{D}_\alpha^2 (\tilde{\mathbf{H}}^B)^H$, substituting which into (43) we observe that the MSE ξ_k is a convex quadratic function of α . Specifically, after some algebraic manipulation and omitting terms that do not depend on α , we obtain

$$\xi_k \propto \alpha^T \Gamma_k \alpha + 2\psi_k^T \alpha, \quad (46)$$

where

$$\Gamma_k \triangleq \operatorname{Re} \{ \mathbf{D}_{\phi_k}^H (\mathbf{H}^U \mathbf{D}_\rho (\mathbf{H}^U)^H + \zeta_R^2 \mathbf{I}) \mathbf{D}_{\phi_k} \} \quad (47a)$$

$$\psi_k \triangleq \operatorname{Re} \{ \mathbf{D}_{\phi_k}^H (\mathbf{H}^U \mathbf{D}_\rho (\mathbf{H}^D)^H \mathbf{c}_k - \sqrt{\rho_k} \mathbf{h}_k^U) \}, \quad (47b)$$

with $\phi_k \triangleq (\tilde{\mathbf{H}}^B)^H \mathbf{c}_k$. We further define $\Gamma \triangleq \sum_{k=1}^K \gamma_k \varpi_k \Gamma_k$ and $\psi \triangleq \sum_{k=1}^K \gamma_k \varpi_k \psi_k$. Notice that Γ_k is positive semi-definite (PSD), so is Γ . Now, the optimization of α can be cast as a convex quadratic program (QP) with linear constraints:

$$\begin{aligned} \min_{\alpha} \quad & \frac{1}{2} \alpha^T \Gamma \alpha + \psi^T \alpha \quad (\text{S2}) \\ \text{s.t.} \quad & (\text{C2}), (\text{C3}) \end{aligned}$$

which can be efficiently solved using standard toolboxes.

The overall optimization procedure is summarized in Algorithm 1. Since the objective function of (P2) is continuously differentiable, and a unique minimizer can be found when updating each variable, convergence of the algorithm to a stationary point is guaranteed [36, Prop. 2.7.1].

Repeater Power Constraint: In practice, the repeater gain is also constrained by its maximum power P_{\max}^R . From an implementation perspective, this can be enforced by incorporating the following constraint while updating the repeater gains α by solving (S2):

$$\alpha_n \leq \sqrt{\frac{P_{\max}^R}{\sum_{k=1}^K \rho_k |h_{nk}^U|^2 + \zeta_R^2}}, \quad \forall n. \quad (\text{C5})$$

Notice that this constraint depends on the user powers ρ which may change across iterations. The objective value (i.e., weighted sum-rate) is still guaranteed to converge, as it is monotonically non-decreasing over the iterations, and upper-bounded. However, while the objective function is guaranteed

Algorithm 1 Joint Uplink Optimization

Input: Channels \mathbf{H}^D , \mathbf{H}^B , \mathbf{H}^U ; noise variances ζ_B^2 and ζ_R^2 ; user weights $\{\gamma_k\}$; maximum power P_{\max} ; stopping threshold ϵ ; maximum number of iterations I_{\max}

Initialize: ρ and α satisfying (C1), (C2), (C3)

1: **while** The change in $\sum_{k=1}^K \gamma_k \log \varpi_k$ exceeds ϵ **and** the maximum iteration I_{\max} is not reached **do**

2: $\mathbf{c}_k \leftarrow \sqrt{\rho_k} (\mathbf{H} \mathbf{D}_\rho \mathbf{H}^H + \Sigma)^{-1} \mathbf{h}_k, \forall k$

3: $\varpi_k \leftarrow 1 / (1 - \sqrt{\rho_k} \mathbf{h}_k^H \mathbf{c}_k), \forall k$

4: $\rho_k \leftarrow \min \left\{ P_{\max}, \left(\frac{\gamma_k \varpi_k \mathbf{c}_k^H \mathbf{h}_k}{\sum_{k'=1}^K \gamma_{k'} \varpi_{k'} |c_{k'}^H \mathbf{h}_k|^2} \right)^2 \right\}, \forall k$

5: Update α by solving the convex QP (S2)

6: **end while**

Output: $\{\mathbf{c}_k\}$, ρ , and α

to converge, the optimization variables are not (there could be multiple feasible solutions that give the same objective function value). Having said that, in our experimental results, we observe that the algorithm still converges well under this additional constraint.

C. Signaling Aspects

When optimizing the uplink performance, we assume that the system has access to accurate channel state information (CSI) for all involved communication links, including the direct links, the user-to-repeater (U2R) links, the R2B links, and the inter-repeater (R2R) links. In practice, the CSI has to be acquired through channel estimation and feedback, which can be done in four steps as follows:

- 1) **User Pilot Transmission:** The K users transmit mutually orthogonal pilot sequences, as in conventional uplink channel estimation without repeaters. During this phase, the repeaters only passively receive signals. Using the received pilots, the BS can estimate the direct-link channels, and the repeaters can estimate the U2R channels.
- 1) **Repeater Pilot Transmission:** The N repeaters transmit their pilot signals in turn, while all other repeaters passively receive signals. Upon receiving the pilot from repeater n , the BS estimates the R2B channel and other repeaters estimate the R2R channels.
- 2) **Feedback of R2R and U2R Channels:** The repeaters feed back the estimated R2R and U2R channels to the BS. Notice that for R2R channels, only channel magnitudes are needed; additionally, when using the first stability condition in (C3), i.e., $\alpha_n \sum_{n'=1}^N |h_{nn'}^R| \leq \eta$, each repeater only needs to feed back the sum, $\sum_{n'=1}^N |h_{nn'}^R|$, which is a scalar, to reduce the signaling overhead.
- 3) **Configuration Feedback:** The BS computes the repeater gains $\{\alpha_n\}$ and the transmit powers $\{\rho_k\}$ based on the estimated channels and feeds them back to the repeaters and the users, respectively.

Compared with a conventional cellular system without repeaters, the use of repeaters requires additional signaling overhead, including repeater pilot transmission and the feedback

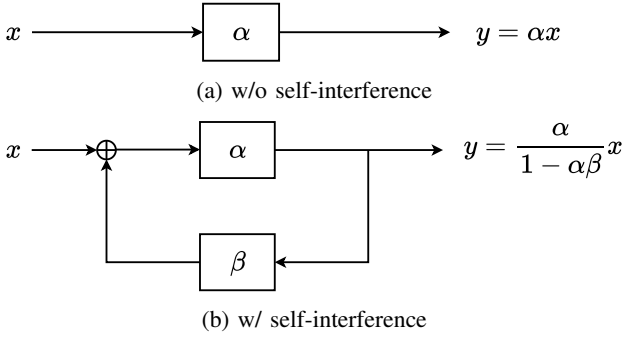


Fig. 8: Repeater response with and without self-interference.

between the repeaters and the BS. However, the repeater gains $\{\alpha_n\}$ are typically fixed for a long duration—reconfiguration is only needed when the large-scale channel statistics change significantly, thereby avoiding excessive overhead. Once the repeater gains are fixed, the system can operate as if the repeaters are transparent. Another potential approach could be to derive an achievable rate lower bound that depends only on the long-term channel statistics, and then optimize the repeater gains directly based on that lower bound, which could be a future direction.

D. Regarding Self-Interference

Typically, when designing full-duplex devices, limiting the self-interference is an important design goal. However, note that the meaning of self-interference is different in the context of full-duplex repeaters than in the context of conventional full-duplex transceivers. In the full-duplex *repeater* case, the repeater transmits *the same signal* as it receives. Hence the effect of self-interference in the repeater case is only a change in effective gain. Our analyses do not exclude self-interference: in (9), the self-interference is included if $h_{nn}^R \neq 0$, and all the results follow regardless of whether self-interference is present.

More specifically, in Fig. 8, we illustrate the effective repeater response without (a) and with (b) self-interference. In either case, the repeater is a linear time-invariant system. In (a), the repeater has a constant amplification gain α , while in (b), the repeater also receives a self-interference signal with loopback gain β . The effective gain then becomes $\alpha/(1 - \alpha\beta)$. While the stability analysis in the paper is directly applicable also when self-interference is present, by replacing α with $\alpha/(1 - \alpha\beta)$, the gain optimization becomes more complicated as the self-interference changes the structure of how the objective depends on α . In particular, self-interference makes the diagonal elements of \mathbf{H}^R non-zero, and the matrix inversion in the overall repeater response in (8) introduces a complicated dependence on α . We have to leave a detailed exploration of this optimization for future work.

VI. NUMERICAL ANALYSIS

The following default setup is used unless otherwise stated. We consider both 6 GHz with 20 MHz bandwidth (referred to as FR1) and 30 GHz with 100 MHz bandwidth (referred to as

FR2), representing two typical frequency bands in 5G NR. The simulation area is circular with radius 1000 meters for FR1 and 500 meters for FR2, where a BS with $M = 64$ antennas is located at the center and $K = 20$ users are placed uniformly at random with 35 meters minimum distance to the BS. $N = 40$ repeaters are placed approximately uniformly using hexagonal packing with 100 meters minimum distance to the BS. We generate the pathloss according to the 3GPP models in [31, Sec. 7.4.1]: the direct and R2B links follow the urban macro (UMa) model, and the U2R and R2R links follow the urban micro (UMi) model. The height of the BS, repeaters, and users are 25, 10, and 1.5 meters, respectively. We assume that LoS components always exist in R2B links;⁷ for other links, the LoS exists probabilistically according to [31, Sec. 7.4.2]. The small-scale fading for non-LoS components is modeled as Rayleigh fading. The BS has an antenna gain of 8 dBi, while the repeaters and users have isotropic antennas. The maximum transmit power of users and repeaters are both set to $P_{\max} = P_{\max}^R = 23$ dBm. The maximum amplification gain of repeaters is $A_{\max} = 90$ dB [13]. At the BS, the noise spectral density is -174 dBm/Hz, and the noise figure is 9 dB. The repeater has the same noise power as the BS, i.e., $\varsigma_R^2/\varsigma_B^2 = 1$. The self-interference is negligible. We ignore the time-delays at repeaters in the simulations (which introduces phase shifts, as explained in Remark 10), while our analysis and optimization framework account for arbitrary time-delays. In Algorithm 1, we use equal user weights (i.e., sum-rate maximization).

Quantitative figures procured from our simulation scenario are: (i) for FR1, the median of received SNR (pre-processing) at the BS from cell-edge user and repeater are -23.4 and -3.9 dB (repeater noise ignored), respectively; and (ii) for FR2, the corresponding SNRs are -32.6 and -15.1 dB, respectively. It can be seen that the cell-edge users experience very poor channel quality in both scenarios, making it difficult for them to perform reliable communication. The SNR further deteriorates in FR2 due to the increased pathloss and noise power resulting from the wider bandwidth.

A. Repeater Placement

To obtain some insights on repeater placement, we consider a scenario where a cell-edge user transmits with full power P_{\max} and a repeater is moved along the line connecting the user and the BS. The large-scale fading coefficients (LSFCs) are denoted by β_D , β_U , and β_B for the direct, U2R, and R2B links, respectively, which are calculated according to the aforementioned pathloss models. The effect of probabilistic LoS is considered for direct and U2R links by taking $\beta = p\beta^{\text{LoS}} + (1-p)\beta^{\text{NLoS}}$, where p is the distance-dependent LoS probability. For an amplification gain α , the received SNR at the BS is $P_{\max}(\beta_D + \alpha^2\beta_U\beta_B)/(\varsigma_B^2 + \alpha^2\beta_U\varsigma_R^2)$, where recall that ς_B^2 and ς_R^2 are the noise power at the BS and repeater, respectively. Compared to the direct-link SNR, $P_{\max}\beta_D/\varsigma_B^2$,

⁷This is an optimistic assumption, and our aim is to show the potential performance gain. In practice, LoS propagation may not always be guaranteed, but should be achieved with a high probability under careful deployment. We have also considered in Sec. VI-C the scenario where the repeaters are arbitrarily deployed so that LoS links can exist with low probability.

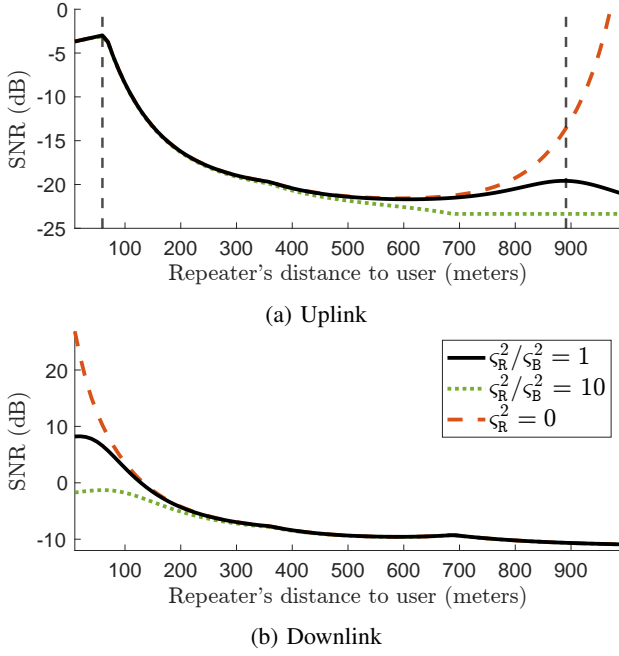


Fig. 9: SNR versus repeater location.

the repeater can improve the SNR by a factor of $\frac{1+\alpha^2\beta_U\beta_B/\beta_D}{1+\alpha^2\beta_U\zeta_R^2/\zeta_B^2}$, which monotonically increases with α^2 when $\beta_U/\zeta_R^2 \geq \beta_D/\zeta_B^2$, and decreases otherwise. This implies that, to maximize the SNR, the repeater amplification gain should be selected as

$$\alpha = \begin{cases} \min \left\{ A_{\max}, \sqrt{\frac{P_{\max}^R}{P_{\max}\beta_U + \zeta_R^2}} \right\}, & \frac{\beta_U}{\zeta_R^2} \geq \frac{\beta_D}{\zeta_B^2} \\ 0, & \text{otherwise.} \end{cases} \quad (48)$$

In Fig. 9a, we plot the uplink SNR at the BS for FR1 when the repeater is placed at different locations along the line connecting the user and the BS under different repeater noise levels. When $\zeta_R^2/\zeta_B^2 = 1$, we observe two transition points—marked by vertical dashed lines—where the SNR trend changes. Before the first transition point, the repeater is too close to the user and the amplification gain is limited by the repeater power constraint. Between the two transition points, the concatenated user-repeater-BS link strength is restricted by the “double pathloss”, i.e., both user-to-repeater and repeater-to-BS links are weak, making the product, $\beta_U\beta_B$, extremely small. Beyond the second transition point, the user-to-repeater SNR, β_U/ζ_R^2 , becomes very low, making it counter-productive to move the repeater further to the BS. Contrarily, in the other two cases: (i) when there is no noise at the repeater ($\zeta_R^2 = 0$), the SNR keeps increasing when moving the repeater closer to the BS; and (ii) when the repeater noise level is high ($\zeta_R^2/\zeta_B^2 = 10$), the repeater has to be turned off if it is too far away from the user, since the signal at the repeater is already too noisy.

The results for downlink are shown in Fig. 9b, where the maximum transmit power of the BS is set to 35 dBm. (The mathematical analysis is similar to uplink, and is therefore omitted.) We observe that, also in the downlink, placing the repeater close to the user is more beneficial. This is because

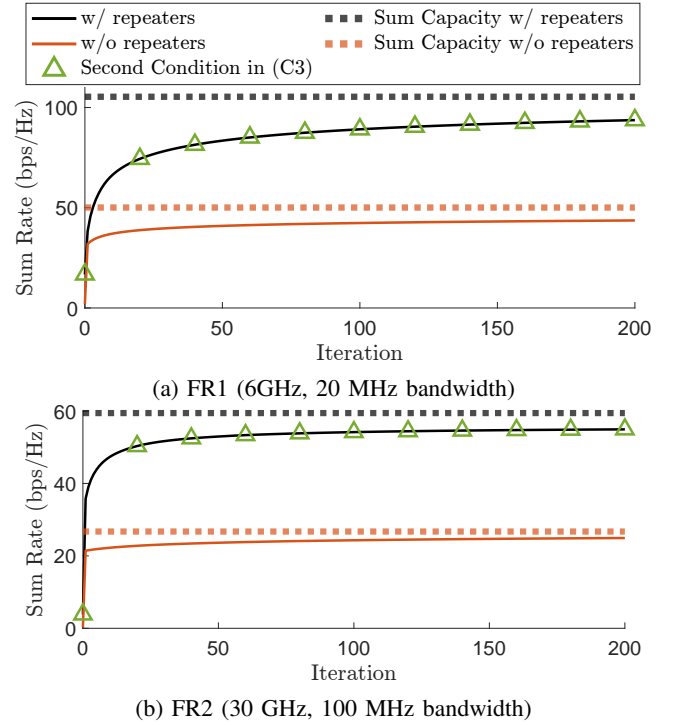


Fig. 10: Convergence of the proposed Algorithm 1.

the BS has much higher transmit power, and a repeater close to the BS can provide little additional gain. Since we consider that the repeaters always have LoS with the BS, it can receive a much stronger signal than the user even at the cell edge.

The above results suggest that the repeaters should be placed such that they receive strong signals from users at the cell edge or coverage holes. When the pathloss information is unknown or time-varying due to mobility, a uniform placement of repeaters is a practical choice, which increases the likelihood of a user having a strong channel to a nearby repeater. Interestingly, such placement in turn maximizes the inter-repeater spacing, enhancing the stability of the repeater swarm.

B. Convergence of the Optimization Algorithm

Next, to demonstrate the convergence of Algorithm 1, we plot the sum rate achieved per iteration in Fig. 10, with or without repeaters (where Line 5 in Algorithm 1 is skipped in the latter case). We choose the first condition in the repeater stability constraint (C3) and set $\eta = 0.9$. (Notice that the result obtained using the second condition in (C3) instead—plotted with triangle markers—is almost identical.) The repeater power constraint (C5) is included when updating the repeater gains. Convergence of the algorithm can be readily observed: the sum rate consistently increases in the beginning and saturates (with a negligible diminishing return) with the progress of iterations. However, more iterations are needed for the algorithm to converge in FR1 compared to FR2. This is because the pathloss is much lower in FR1, and many more communication links have non-negligible effects. To balance complexity and performance, we henceforth set the maximum number of iterations to $I_{\max} = 50$, and enable early stopping

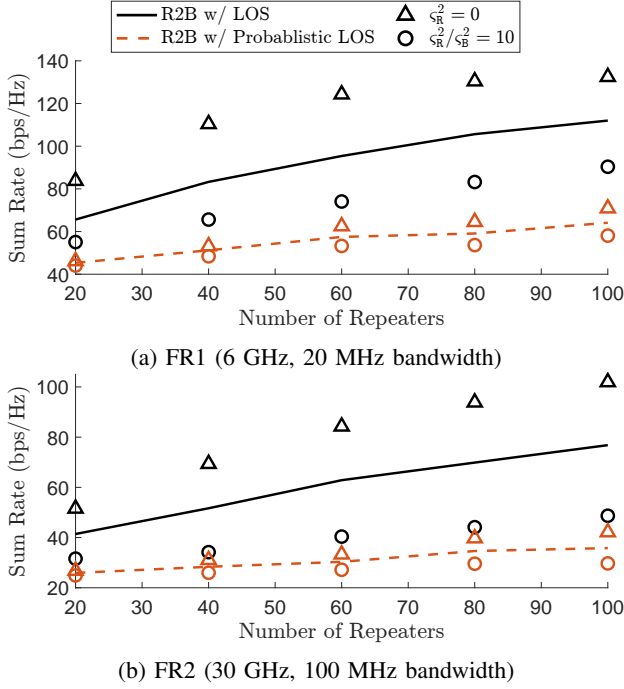


Fig. 11: Sum rate versus number of repeaters.

if the sum rate improvement is less than $\epsilon = 10^{-3}$ bps/Hz between consecutive iterations for the simulation results. As a reference, we also plot the sum capacity in (37) using the repeater gains obtained after the algorithm converges. Note that the repeater gains are optimized for sum rate, which do not necessarily maximize the sum capacity—nevertheless, this should work reasonably well, as we observe that the achieved sum rate is quite close to the sum capacity.

C. Number of Repeaters

The achieved sum rate with different number of repeaters is plotted in Fig. 11. Particularly, we compare the results with the case where LoS exists only probabilistically in the repeater-to-BS links (notice that the LoS probability is already less than 5% when the repeater is 400 meters away from the BS). As observed, the performance gains from repeaters are largely negated when the LoS cannot be guaranteed. It is necessary to ensure that the repeaters always have strong channels to the BS through careful placement. The noise power at the repeater is also a critical factor, as the performance deteriorates significantly when the repeater noise level is very high.

In Fig. 12, we plot the cumulative distribution function (CDF) of individual user rates with different numbers of repeaters. As observed, a denser repeater deployment provides a more uniform rate distribution among users, as even cell-edge users can achieve an improved rate with one or more repeaters in the vicinity. We also observe an “implicit scheduling” effect (a small portion, $\approx 2.5\%$, of users have zero transmit power) when the number of repeaters is not so large. This is because when two users are equally close to an isotropic-antenna repeater, they cause strong interference to each other if both transmit (please recall the example in Sec. II). Since the chosen

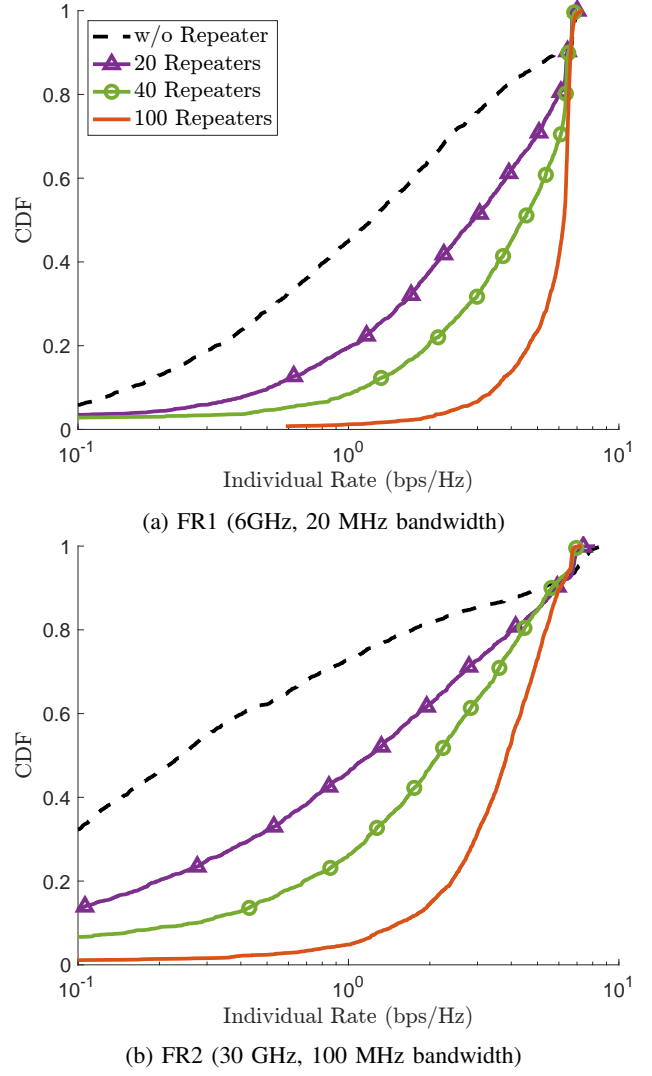


Fig. 12: Individual rate distribution.

optimization criterion is sum-rate maximization, one user may be silenced for the other to transmit more effectively. However, this should not be a significant issue due to the following reasons: (i) compared to the case without repeaters, the number of users with very low rates (e.g., less than 0.1 bps/Hz) is still less; (ii) the problem can be avoided by user scheduling, which is always implemented in the systems and will not require much additional overhead due to the small number of affected users; (iii) although short-term fairness may be compromised, sum-rate maximization still provides long-term fairness, as the user location will change over time; and (iv) users with high quality-of-service requirements can be prioritized by assigning them higher weights in the optimization. Alternatively, one could consider different optimization criteria (e.g., max-min fairness) or use more advanced multi-antenna repeaters for spatial separability, which is beyond the scope of this paper.

D. Impact of Stability Margin η

In the stability condition (C3), we introduced a stability margin η to provide robust stability under channel uncertainties. It

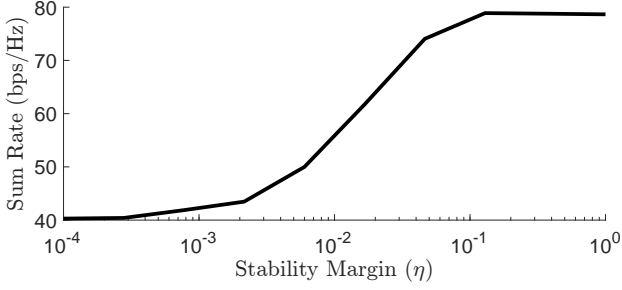


Fig. 13: Impact of the stability margin η .

is clear that a smaller η leads to a more conservative stability condition, which may limit the amplification gain of repeaters and, consequently, the achievable sum rate. Ideally, η should be chosen such that the impact of inter-repeater interaction can be sufficiently mitigated, while not being too conservative to avoid unnecessary performance loss. Unfortunately, it is not straightforward to accurately analyze the impact of η on the sum rate. Instead, in Fig. 13, we numerically investigate the impact of η on the sum rate in FR1. We observe that the result is not sensitive to the choice of η as long as it is not too small (e.g., $\eta < 0.1$). However, we have to note that the results depend on the chosen simulation setup, and may vary in different scenarios.

VII. CONCLUDING REMARKS

Deploying swarms of low-cost, low-complexity, and low-power repeaters is a promising solution to improve coverage and channel rank in cellular networks. For example, in our tested scenario, deploying 40 single-antenna repeaters—each with the same power budget as user devices—within a cell of 1000 meters radius can nearly double the sum rate compared to the case without repeaters.

However, to achieve the full potential of the envisioned repeater swarm-assisted cellular system, careful system design and optimization are necessary. First, repeaters inject additional noise and interference. Second, interaction instability caused by the positive feedback between repeaters must be avoided—this can be guaranteed by verifying the sufficient conditions for stability that we derived; these conditions depend only on the inter-repeater channel amplitudes. Third, the repeaters should be placed close to the users that require assistance, for example, at the cell edge and coverage holes, to combat the “double pathloss” effect and the injected noise. Preferably, the repeaters should have strong LoS channels to the BS through careful placement.

Considering multi-cell scenarios with imperfect channel state information and pilot contamination can be of interest for future study. Other potential directions include generalization to time-varying systems, the optimization of repeater time-delays, more effective signaling schemes, a deeper analysis of self-interference, and the use of multi-antenna repeaters to enhance spatial separability.

APPENDIX

PROOF OF THEOREM 1

Conditions for the existence of a unique and causal impulse response are provided in [37, Th. 28.2], and the condition for the bounded-energy stability is given in [26, Th. 4.3]. Our proof idea is to show that—under the conditions imposed in Theorem 1—the requirements of both theorems are satisfied for our particular system.

Instead of $G(s)$, we consider the transfer function matrix

$$\begin{aligned} Z(s) &= G(s) - D_{a(s)} \\ &= (I - D_{a(s)} H^R(s))^{-1} D_{a(s)} H^R(s) D_{a(s)}. \end{aligned} \quad (49)$$

Since the system $D_{a(s)}$ is causal and stable (each diagonal element represents a finite amplification with delay), $G(s)$ is causal and stable if and only if $Z(s)$ is causal and stable.

To proceed, we prove the following lemma.

Lemma 1. *Under Assumptions 1 and 2, if the image of $\det(I - D_{a(j\omega)} H^R(j\omega))$ does not encircle the origin, then*

- (a) $Z(s)$ is analytic in \mathbb{C}_+
- (b) All elements of $Z(s)$ converges to 0 as $|s| \rightarrow \infty$ in \mathbb{C}_+
- (c) All elements of $Z(s)$ are absolutely integrable on all vertical lines in \mathbb{C}_+ .

Proof: (a) Since both $H^R(s)$ and $D_{a(s)}$ are analytic in \mathbb{C}_+ and the determinant of a matrix involves only sums and products (both of which preserve analyticity) of its elements, $\det(I_N - D_{a(j\omega)} H^R(j\omega))$ is analytic in \mathbb{C}_+ and, therefore, has no pole in \mathbb{C}_+ . Consider the Nyquist contour, consisting of a path traveling up the $j\omega$ axis, from $0 - j\infty$ to $0 + j\infty$, along with a semicircular arc in \mathbb{C}_+ of infinitely large radius that starts at $0 + j\infty$ and travels clockwise to $0 - j\infty$, enclosing the entire \mathbb{C}_+ . According to Cauchy’s argument principle [38, pp. 230], the difference between the number of zeros and poles of $\det(I_N - D_{a(s)} H^R(s))$ within \mathbb{C}_+ equals the number of clockwise encirclements of the origin traced by its image as s traverses the Nyquist contour in a clockwise direction. Since $\det(I_N - D_{a(s)} H^R(s))$ has no poles in \mathbb{C}_+ , the number of encirclements of the origin equals the number of zeros. Furthermore, under Assumption 2, $|h_{nn'}(s)| \rightarrow 0$ as $|s| \rightarrow 0$ in \mathbb{C}_+ , meaning that on the semicircular part of the contour, the image of $\det(I_N - D_{a(s)} H^R(s))$ collapses to a single point at $1 + j0$. Thus, if the image of $\det(I_N - D_{a(j\omega)} H^R(j\omega))$ does not encircle the origin, it follows that $\det(I_N - D_{a(s)} H^R(s))$ has no zero in \mathbb{C}_+ , and we have

$$(I_N - D_{a(s)} H^R(s))^{-1} = \frac{\text{adj}(I_N - D_{a(s)} H^R(s))}{\det(I_N - D_{a(s)} H^R(s))}. \quad (50)$$

Since all elements in the adjugate matrix are determinants of some sub-matrices (possibly with sign changes), the adjugate matrix $\text{adj}(I_N - D_{a(s)} H^R(s))$ is also analytic in \mathbb{C}_+ . As division preserves analyticity when the denominator is nonzero, we have that $(I_N - D_{a(s)} H^R(s))^{-1}$ is analytic in \mathbb{C}_+ . Then, from (49), we have that $Z(s)$ is analytic in \mathbb{C}_+ .

(b)-(c) For an arbitrary matrix X , we denote by $\sigma_n(X)$ the n th singular value, by $\sigma_{\min}(X)$ the smallest singular value, by $\|X\|_2$ the spectral norm (i.e., the largest singular value),

and by $\|\mathbf{X}\|_\infty$ the maximum magnitude of its elements (i.e., the ℓ_∞ vector norm applied after vectorizing \mathbf{X}). For $|s| > \delta$ in \mathbb{C}_+ , all singular values of $\mathbf{I} - \mathbf{D}_{\mathbf{a}(s)}\mathbf{H}^R(s)$ satisfy

$$\begin{aligned} |\sigma_n(\mathbf{I} - \mathbf{D}_{\mathbf{a}(s)}\mathbf{H}^R(s)) - 1| &\leq \|\mathbf{D}_{\mathbf{a}(s)}\mathbf{H}^R(s)\|_2 \\ &\leq N \|\mathbf{D}_{\mathbf{a}(s)}\mathbf{H}^R(s)\|_\infty \\ &\leq \frac{NCA}{|s|^{1+\varepsilon}}, \end{aligned} \quad (51)$$

where $A \triangleq \max_n \alpha_n$ is the maximum amplification gain among all repeaters. In (51), the first inequality follows from [29, Cor. 7.3.5], the second inequality from $\|\mathbf{X}\|_2 \leq N \|\mathbf{X}\|_\infty$ [29, pp. 365], and the last inequality from Assumption 2. From (51), we have

$$\sigma_{\min}(\mathbf{I} - \mathbf{D}_{\mathbf{a}(s)}\mathbf{H}^R(s)) \geq 1 - \frac{NCA}{|s|^{1+\varepsilon}}. \quad (52)$$

Thus, for $|s| \geq \delta' \triangleq \max\{\delta, (2NCA)^{\frac{1}{1+\varepsilon}}\}$ in \mathbb{C}_+ ,

$$\begin{aligned} \left\|(\mathbf{I} - \mathbf{D}_{\mathbf{a}(s)}\mathbf{H}^R(s))^{-1}\right\|_\infty &\leq \left\|(\mathbf{I} - \mathbf{D}_{\mathbf{a}(s)}\mathbf{H}^R(s))^{-1}\right\|_2 \\ &= \frac{1}{\sigma_{\min}(\mathbf{I} - \mathbf{D}_{\mathbf{a}(s)}\mathbf{H}^R(s))} \\ &\leq \frac{1}{1 - \frac{NCA}{|s|^{1+\varepsilon}}} \\ &\leq 1 + \frac{2NCA}{|s|^{1+\varepsilon}}, \end{aligned} \quad (53)$$

where the first inequality follows from $\|\cdot\|_\infty \leq \|\cdot\|_2$ [29, pp. 365], the second inequality from (52), and the last inequality is obtained by applying the inequality $\frac{1}{1-x} = 1 + \frac{x}{1-x} \leq 1 + 2x$ with $x = \frac{NCA}{|s|^{1+\varepsilon}} \in (0, \frac{1}{2})$ which holds if $|s| \geq (2NCA)^{\frac{1}{1+\varepsilon}}$. Now, for $|s| \geq \delta'$ in \mathbb{C}_+ , we have

$$\begin{aligned} \|\mathbf{Z}(s)\|_\infty &= \left\|(\mathbf{I} - \mathbf{D}_{\mathbf{a}(s)}\mathbf{H}^R(s))^{-1} \mathbf{D}_{\mathbf{a}(s)}\mathbf{H}^R(s) \mathbf{D}_{\mathbf{a}(s)}\right\|_\infty \\ &\leq N \left\|(\mathbf{I} - \mathbf{D}_{\mathbf{a}(s)}\mathbf{H}^R(s))^{-1}\right\|_\infty \|\mathbf{D}_{\mathbf{a}(s)}\mathbf{H}^R(s) \mathbf{D}_{\mathbf{a}(s)}\|_\infty \\ &\leq N \left(1 + \frac{2NCA}{|s|^{1+\varepsilon}}\right) \frac{CA^2}{|s|^{1+\varepsilon}} \\ &= \frac{NCA^2}{|s|^{1+\varepsilon}} + \frac{2N^2C^2A^3}{|s|^{2+2\varepsilon}}, \end{aligned} \quad (54)$$

where the first inequality is due to the fact that $N \|\cdot\|_\infty$ is a matrix norm and satisfies the submultiplicativity property, and the second inequality can be obtained by applying (53) and Assumption 2. From (54), it follows that $\|\mathbf{Z}(s)\|_\infty$ converges to 0 as $|s| \rightarrow \infty$ in \mathbb{C}_+ and

$$\int_{-\infty}^{-\delta'} \|\mathbf{Z}(\sigma + j\omega)\|_\infty d\omega + \int_{\delta'}^{\infty} \|\mathbf{Z}(\sigma + j\omega)\|_\infty d\omega < \infty.$$

From (a), we have that $\mathbf{Z}(s)$ is analytic in \mathbb{C}_+ ; therefore,

$$\int_{-\delta'}^{\delta'} \|\mathbf{Z}(\sigma + j\omega)\|_\infty d\omega < \infty.$$

Combining the above results, we conclude that all elements of $\mathbf{Z}(s)$ are absolutely integrable on all vertical lines in \mathbb{C}_+ . ■

When all the assertions in Lemma 1 hold, it follows from [37, Th. 28.2] that $\mathbf{Z}(s)$ represents the Laplace transform of the impulse response

$$\mathbf{Z}(t) \triangleq \frac{1}{j2\pi} \int_{\sigma-j\infty}^{\sigma+j\infty} \mathbf{Z}(s) e^{st} ds, \quad (55)$$

which is unique, i.e., the integral is independent of the choice of σ when $\sigma \geq 0$, and causal, i.e., $\mathbf{Z}(t) = \mathbf{0}$ for $t < 0$.

Furthermore, $\mathbf{Z}(s)$ has a finite \mathcal{H}_∞ norm, i.e.,

$$\|\mathbf{Z}\|_{\mathcal{H}_\infty} \triangleq \sup_{\operatorname{Re}\{s\} > 0} \|\mathbf{Z}(s)\|_2 < \infty, \quad (56)$$

since $\mathbf{Z}(s)$ is analytic in \mathbb{C}_+ and $\|\mathbf{Z}(s)\|_\infty$ converges to zero as $|s| \rightarrow \infty$ in \mathbb{C}_+ . According to [26, Th. 4.3], $\mathbf{Z}(t)$ is bounded energy stable when $\|\mathbf{Z}\|_{\mathcal{H}_\infty}$ is finite. As previously mentioned, $\mathbf{G}(s)$ shares the same stability properties as $\mathbf{Z}(s)$, which completes the proof.

REFERENCES

- [1] E. G. Larsson and J. Bai, "Stability analysis of interacting wireless repeaters," in *Proc. 25th Int. Workshop Signal Process. Advances Wireless Commun. (SPAWC)*, Sep. 2024, pp. 756–760.
- [2] E. G. Larsson, O. Edfors, F. Tufvesson, and T. L. Marzetta, "Massive MIMO for next generation wireless systems," *IEEE Comm. Mag.*, vol. 52, no. 2, pp. 186–195, Feb. 2014.
- [3] H. Q. Ngo, A. Ashikhmin, H. Yang, E. G. Larsson, and T. L. Marzetta, "Cell-free massive MIMO versus small cells," *IEEE Trans. Wireless Commun.*, vol. 16, no. 3, pp. 1834–1850, Mar. 2017.
- [4] S. Willhammar, H. Iimori, J. Vieira, L. Sundström, F. Tufvesson, and E. G. Larsson, "Achieving distributed MIMO performance with repeater-assisted cellular massive MIMO," *IEEE Commun. Mag.*, vol. 63, no. 3, pp. 114–119, Mar. 2025.
- [5] M. N. Patwary, P. B. Rapajic, and I. Oppermann, "Capacity and coverage increase with repeaters in UMTS urban cellular mobile communication environment," *IEEE Trans. Commun.*, vol. 53, no. 10, pp. 1620–1624, Oct. 2005.
- [6] S. K. Sharma, M. Patwary, S. Chatzinotas, B. Ottersten, and M. Abdel-Maguid, "Repeater for 5G wireless: A complementary contender for spectrum sensing intelligence," in *Proc. IEEE Int. Conf. Commun.*, Jun. 2015, pp. 1416–1421.
- [7] M. Garcia-Lozano, L. Alonso, F. Casadevall, S. Ruiz, and L. M. Correia, "Enhanced analysis of WCDMA networks with repeaters deployment," *IEEE Trans. Wireless Commun.*, vol. 6, no. 9, pp. 3429–3439, Sep. 2007.
- [8] L.-S. Tsai and D.-S. Shiu, "Capacity scaling and coverage for repeater-aided MIMO systems in line-of-sight environments," *IEEE Trans. Wireless Commun.*, vol. 9, no. 5, pp. 1617–1627, May 2010.
- [9] Y. Ma, D. Zhu, B. Li, and P. Liang, "Channel estimation error and beam-forming performance in repeater-enhanced massive MIMO systems," in *Proc. IEEE 26th Annu. Int. Symp. Pers., Indoor, Mobile Radio Commun. (PIMRC)*, Aug. 2015, pp. 672–677.
- [10] M. Lerch, P. Svoboda, J. Resch, and M. Rupp, "Cellular uplink impairments in vehicular repeater deployments," *IEEE Open J. Veh. Technol.*, vol. 6, pp. 487–501, Jan. 2025.
- [11] L. Eller, P. Svoboda, and M. Rupp, "A differentiable throughput model for load-aware cellular network optimization through gradient descent," *IEEE Access*, vol. 12, pp. 14 547–14 562, Feb. 2024.
- [12] 3GPP, "NR repeater radio transmission and reception," TS 38.106, 2022.
- [13] F. Carvalho *et al.*, "Network-controlled repeater—An introduction," *IEEE Commun. Stand. Mag.*, pp. 1–1, 2025.
- [14] M. Kapuruhamy *et al.*, "Understanding the 3GPP standardization aspects of network-controlled repeaters," *IEEE Commun. Mag.*, vol. 9, no. 1, pp. 36–43, Mar. 2025.
- [15] G. C. Da Silva *et al.*, "Impact of network deployment on the performance of NCR-assisted networks," in *Proc. 19th IEEE Int. Symp. Wireless Commun. Syst. (ISWCS)*, Jul. 2024.
- [16] C.-K. Wen, L.-S. Tsai, A. Shojaeifard, P.-K. Liao, K.-K. Wong, and C.-B. Chae, "Shaping a smarter electromagnetic landscape: IAB, NCR, and RIS in 5G standard and future 6G," *IEEE Commun. Stand. Mag.*, vol. 8, no. 1, pp. 72–78, Mar. 2024.

- [17] R. A. Ayoubi, M. Mizmizi, D. Tagliaferri, D. D. Donno, and U. Spagnolini, "Network-controlled repeaters vs. reconfigurable intelligent surfaces for 6G mmW coverage extension: A simulative comparison," in *Proc. IEEE 21st Mediterranean Commun. Comput. Netw. Conf.*, Jun. 2023, pp. 196–202.
- [18] G. Leone, E. Moro, I. Filippini, A. Capone, and D. D. Donno, "Towards reliable mmWave 6G RAN: Reconfigurable surfaces, smart repeaters, or both?" in *Proc. IEEE 20th Int. Symp. Model. Optim. Mobile, Ad hoc, Wireless Netw.*, Sep. 2022, pp. 81–88.
- [19] M. Åström, P. Gentner, O. Haliloglu, B. Makki, and O. Tageman, "RIS in cellular networks—Challenges and issues," *IEEE Access*, vol. 13, pp. 129 269–129 283, 2025.
- [20] G. da Silva *et al.*, "Cellular network densification: A system-level analysis with IAB, NCR and RIS," *arXiv preprint arXiv:2410.02415*, 2024.
- [21] R. Aghazadeh Ayoubi, M. Mizmizi, E. Moro, I. Filippini, and U. Spagnolini, "Advanced network planning in 6G smart radio environments," *arXiv preprint arXiv:2411.06021*, 2024.
- [22] R. A. Ayoubi, E. Moro, M. Mizmizi, D. Tagliaferri, I. Filippini, and U. Spagnolini, "Optimal planning for heterogeneous smart radio environments," *IEEE Trans. Mobile Comput.*, pp. 1–16, 2025.
- [23] H. Guo *et al.*, "A comparison between network-controlled repeaters and reconfigurable intelligent surfaces," *arXiv preprint arXiv:2211.06974*, 2022.
- [24] O. A. Topal, O. T. Demir, E. Björnson, and C. Cavdar, "Fair and energy-efficient activation control mechanisms for repeater-assisted massive MIMO," 2025. [Online]. Available: <https://arxiv.org/abs/2504.03428>
- [25] E. G. Larsson, J. Vieira, and P. Frenger, "Reciprocity calibration of dual-antenna repeaters," *IEEE Wireless Commun. Lett.*, vol. 13, no. 6, pp. 1606–1610, Jun. 2024.
- [26] K. Zhou and J. C. Doyle, *Essentials of robust control*. Prentice hall Upper Saddle River, NJ, 1998, vol. 104.
- [27] S. Skogestad and I. Postlethwaite, *Multivariable Feedback Control: Analysis and Design*. John Wiley & Sons, 2005.
- [28] Y. Chait, C. Maccluer, and C. J. Radcliffe, "A Nyquist stability criterion for distributed parameter systems," *IEEE Trans. Autom. Control*, vol. 34, no. 1, pp. 90–92, Jan. 1989.
- [29] R. A. Horn and C. R. Johnson, *Matrix Analysis*. Cambridge University Press, 2012.
- [30] J. M. Maciejowski, *Multivariable Feedback Design*. Addison-Wesley Publishing Company, 1989.
- [31] 3GPP, "Study on channel model for frequencies from 0.5 to 100 GHz," TR 38.901, 2024.
- [32] S. Shi, M. Schubert, and H. Boche, "Downlink MMSE transceiver optimization for multiuser MIMO systems: Duality and sum-MSE minimization," *IEEE Trans. Signal Process.*, vol. 55, no. 11, pp. 5436–5446, Nov. 2007.
- [33] M. K. Varanasi and T. Guess, "Optimum decision feedback multiuser equalization with successive decoding achieves the total capacity of the Gaussian multiple-access channel," in *Proc. 31th Asilomar Conf. Signals, Syst. and Comput.*, 1997, pp. 1405–1409.
- [34] E. Björnson, J. Hoydis, and L. Sanguinetti, "Massive MIMO networks: Spectral, energy, and hardware efficiency," *Foundations and Trends® in Signal Processing*, vol. 11, no. 3-4, pp. 154–655, 2017.
- [35] Q. Shi, M. Razaviyayn, Z.-Q. Luo, and C. He, "An iteratively weighted MMSE approach to distributed sum-utility maximization for a MIMO interfering broadcast channel," *IEEE Trans. Signal Process.*, vol. 59, no. 9, pp. 4331–4340, Sep. 2011.
- [36] D. P. Bertsekas, "Nonlinear Programming," *J. Oper. Res. Soc.*, vol. 48, no. 3, pp. 334–334, 1997.
- [37] G. Doetsch, *Introduction to the Theory and Application of the Laplace Transformation*. Springer Science & Business Media, 2012.
- [38] J. W. Brown and R. V. Churchill, *Complex Variables and Applications*. McGraw-Hill, 2009.